ANALYSIS OF THE FLEXURAL RUPTURE LIMIT STATE FOR STEEL CONNECTIONS UTILIZING A FIBER ANALYSIS

By

Kaitlin Casey

Graduate Technical Project Report

This Graduate Project is for Partial Fulfillment of Requirements for the Degree of

Master of Science in Architectural Engineering

at

Lawrence Technological University

Department of Civil and Architectural Engineering

Southfield, MI

July 2023

ABSTRACT

Steel bolted plate connections are often subjected to flexure, in which the plate must be analyzed considering the effects of eccentricity and multiple limit states. These limit states include yielding, lateral-torsional buckling, local buckling, and flexural rupture. Calculations for analyzing these limit states are defined within the AISC Steel Design Manual Part 9: Design of Connecting Elements (AISC, 2017). The limit state of flexural rupture equation has changed in the AISC Steel Design Manual over time and the current version of the equation seems to be flawed in its assumption that the entire cross-section reaches the ultimate stress of the plate material when flexural rupture occurs. The intent of this report is to discover the actual behavior of a plate section up to the point of flexural rupture using a fiber-based model, and to compare those results with the current flexural rupture capacity equation to determine its accuracy.

Twenty-four test configurations were analyzed using fiber-based models and using an idealized yet realistic stress-strain profile for the material, which assumes A36 steel. The configurations were comprised of 3, 4, or 5 bolt rows, 7/8 inch or 1 inch bolt diameters, standard or oversized bolt holes, and practical or minimum spacing and edge distances values. After the completion of the fiber-based model analysis for all test configurations, the resulting capacities were compared to each of the flexural rupture equations.

Although the stress profile in the cross-section is unrealistic, the analytical results determined that the current AISC flexural rupture equation is reasonably accurate in predicting the flexural moment capacity of a given plate configuration. This is primarily because enough of the material farthest from the neutral axis reaches the ultimate stress or close to it when failure is assumed to occur, and this material contributes the most to the corresponding internal moment. In all test specimens, the current flexural rupture equation overpredicted the actual moment

capacity as found in the fiber-base models by less than 5%. When using this equation in LRFD applications, the equation is paired with a resistance factor of 0.75 which compensates for the overprediction and it can be determined that this equation can be used without apprehension.

Advisor: Dr. Keith Kowalkowski Date 7/17/2023

Associate Professor and Assistant Chair

Department of Civil and Architectural Engineering

Lawrence Technological University

TABLE OF CONTENTS

LIST OF FIGURES

LIST OF TABLES

CHAPTER 1: INTRODUCTION AND BACKGROUND

1.1 Introduction

Structural systems are inherently made up of multiple connecting members designed to transfer real world loading conditions from the outermost members into the foundations as safely and efficiently as possible. It is imperative that each member and member connection is accurately designed and sized to have a capacity that meets or exceeds the assumed loading requirements. The connections must be designed to be able to effectively transfer the loads from one member to the next. As connection design can be complex, there are instances where an eccentricity is designed for within a connection, causing flexure within the connecting element.

There are multiple design limit states that must be considered to assure that a flexural connection design can successfully withstand and transfer the necessary loads. Information on design capacity for each of the limit states is available in the AISC Specification for Structural Steel Buildings, Section J4.5 446-16.1 (AISC, 2017). The limit states for affected and connecting elements subject to flexure are discussed in AISC Steel Manual Part 9: Design of Connecting Elements (AISC, 2016), and are described as follows:

- Yielding - considers the maximum moment capacity of the connecting section given specific dimensional limitations
- Lateral-Torsional Buckling - considers unrestrained elements subjected to loading away from its longitudinal axis as well as twisting
- Local Buckling - considers slender elements that may warp along their longitudinal axis before yielding
- Rupture - considers the maximum flexural capacity of the connecting section given specific dimensional limitations for extended configurations

This report will discuss the failure mode of flexural rupture as seen in extended shear tab connection configurations. These connections are defined by a specific set of dimensional limitations discussed in the AISC Single-Plate Connections 10-89 (AISC, 2016) and are illustrated below. While the conventional configuration (as shown in Figure 1) is limited in the dimensional properties of the plate and bolts, the extended configuration (as shown in Figure 2) is less limited in these and other properties, allowing a more diverse and extreme range of specimen variations for this report.

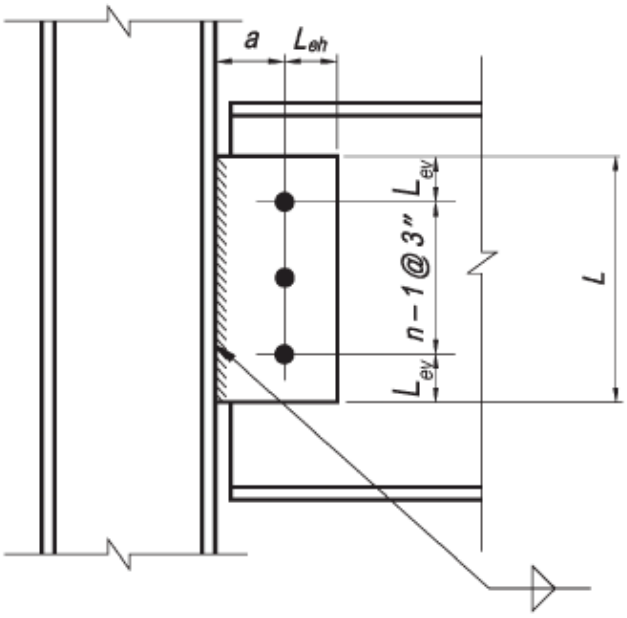

Figure 1 : A Single-Plate Connection-Conventional Configuration (AISC, 2016)

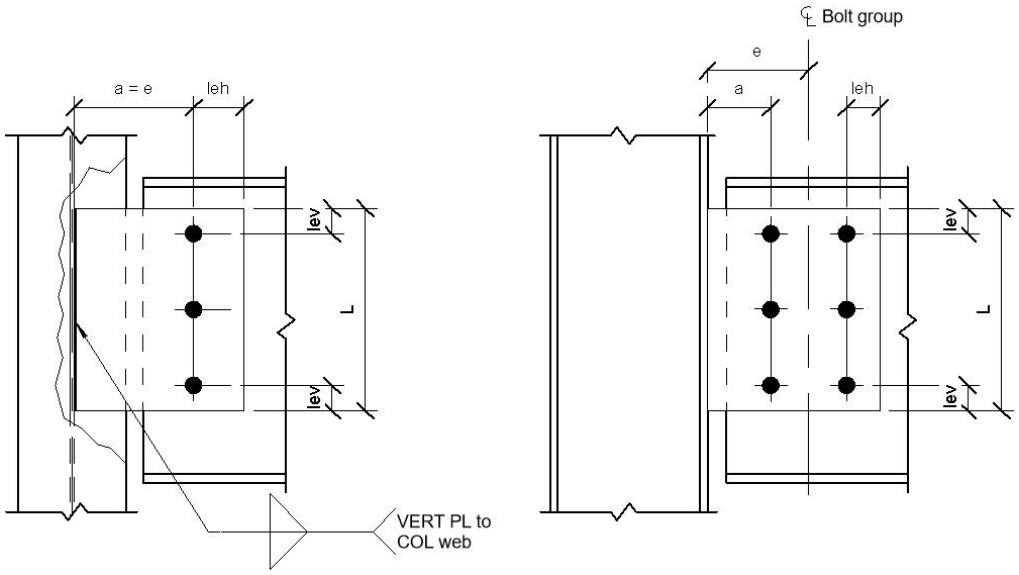

Figure 2: Single-Plate Connection-Extended Configuration (AISC, 2016)

As shown in Figure 1 and Figure 2, "a" represents the distance from the weld line to the bolt line. If this distance is less than 3.5 inches, and there is only one column of bolts (as shown in Figure 1), then eccentricity does not need to be considered, which limits the amount of connection design calculations that need to be performed. In all other conditions, the shear tab and bolts must be designed as eccentric and the extended configuration (Figure 2) procedure must be used and the flexural rupture limit for the plate needs to be considered.

1.2 Background

The American Institute of Steel Construction (AISC) has published design and construction reference manuals for structural steel since 1927. The first nine editions of the "Manual of Steel Construction" were based under the design philosophy called Allowable Stress Design, and are often referred to as the "old ASD manuals." After the ninth edition manual was released in 1989, there was a shift in design philosophy from Allowable Stress Design to Allowable Strength Design and Load and Resistance Factor Design. The AISC Committees converted the earlier equations from elastic to plastic under the assumption that the other limiting states, such as buckling and shear rupture, were properly addressed. This created a set of

intermediary manuals called “Manual of Steel Construction: Load and Resistance Factor Design”. After the publication of these manuals finished with the third edition in 2001, the series continued with the “Manual of Steel Construction” thirteenth edition, published in 2005. All manuals previous to this 2005 publication are officially out-of-print.

Before the shift in design philosophy occurred, the flexural rupture limit capacity equation was initially defined in the AISC Ninth Edition Manual of Steel Construction: Allowable Stress Design (AISC, 1989) as shown in Equation 1-1.

$$\boldsymbol{M_n = F_y S_{net}} \qquad \textbf{Equation (1 - 1)}$$

In Equation 1-1, F_y is equal to the yield strength of the steel and S_{net} is the net elastic section modulus. This formula assumes that the entire net cross-section is behaving elastically, with a linear distribution of stress in the net cross-section, and the point farthest away from the neutral axis just reaching the yield stress.

Towards the end of the transition from the “old ASD” design philosophy to the “new ASD and LRFD” approach, the “Manual of Steel Construction: Load and Resistance Factor Design” third edition was created (AISC, 2001). In this edition, the revised flexural rupture equation is defined as follows:

$$\boldsymbol{M_n = F_u S_{net}} \qquad \textbf{Equation (1 - 2)}$$

In Equation 1-2 and in comparison to Equation 1-1, the yield strength, F_y, was replaced with the ultimate strength, F_u, while the elastic section modulus, S_{net}, is still as it was in Equation 1-1. This revised equation shows a relationship that incorporates both elastic and plastic properties into one capacity limit state. Inherently, the equation implies a stress distribution in the cross-section that is not realistic.

A second revision to the flexural rupture limit equation was implemented in the thirteenth edition of the "Steel Construction Manual" published in 2005 (AISC, 2005). In this revision, the new flexural rupture limit equation is given as Equation 1-3.

$$\boldsymbol{M_n = F_u Z_{net}} \qquad \textbf{Equation (1 - 3)}$$

Comparing Equation 1-3 to Equation 1-2, the previously used ultimate strength remained intact, while the elastic section modulus, S_{net}, is replaced by the plastic section modulus, Z_{net}. Using Z_{net} implies that the new and currently used equation for flexural rupture assumes that the entire net cross-section (gross cross-section minus the bolt holes) reaches the ultimate stress in either tension or compression when a failure mechanism occurs.

It is also worth noting that the AISC Commentary for Section J4.5 (AISC, 2017) discusses the Strength of Elements in Flexure and describes that the "available flexural strength of connecting elements in LRFD can be calculated as the minimum of $0.9F_yZ_{gross}$ and $0.75F_uZ_{net}$ or in ASD as the minimum of $F_yZ_{gross}/1.67$ and $F_uZ_{net}/2.00$". It is also mentioned here that "[i]f deflection is a concern, the factored loads should also be checked against $0.9F_yS_{gross}$ (Mohr and Murray, 2008)". These equations are a result of experimentation done by Mohr and Murray (2008) and were created to verify the accuracy of the flexural rupture equation. This experiment will be discussed later in this report. These equations consider safety factors as well as different assumptions as to the elasticity or plasticity of the cross-section and material strength.

In order to analytically examine the various forms of the flexural rupture equation, a fiber-based model will be created. This method of analysis uses the actual stress-strain curve of a material to determine the stresses present at various depths, or fibers, within the member cross-section. Although the typical stress-strain curve for steel is assumed to similar to Figure 3, the

actual stress-strain curve can vary, meaning that the typical values (or design minimum values from AISC (2017)) used for the yield strength and ultimate strength of a given steel type are not necessarily representative of reality.

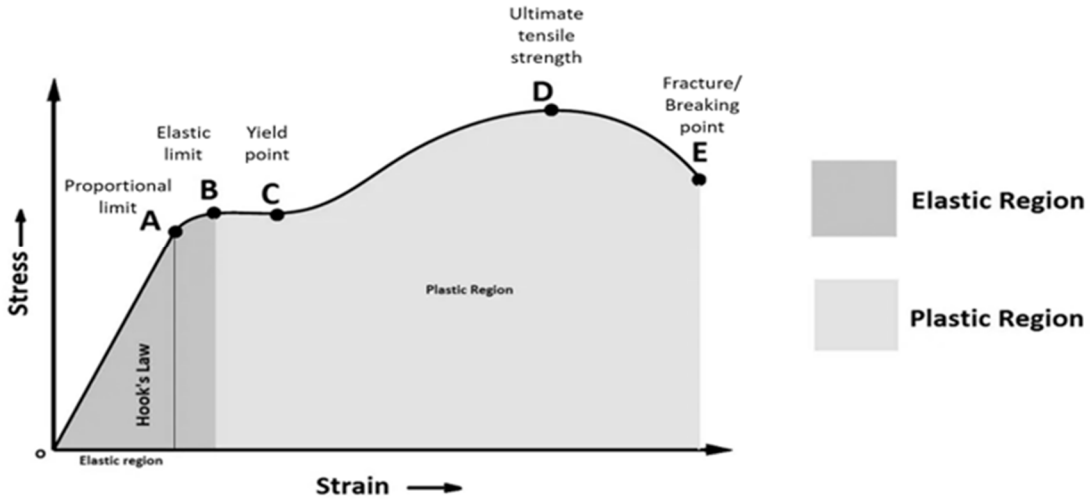

Figure 3: Example of a Stress-Strain Curve for Steel (Stress-Strain Curve)

Figure 4 shows the stress distribution in the plate cross-section under the various flexural rupture equation assumptions. The accuracy of the assumed values from the stress-strain curve and how they act upon the cross-section is important in predicting the behavior of a connection in flexure. As shown, the realistic behavior of a cross-section undergoing flexure should theoretically be non-linear and is somewhere between the equations that make use of the ultimate tensile strength.

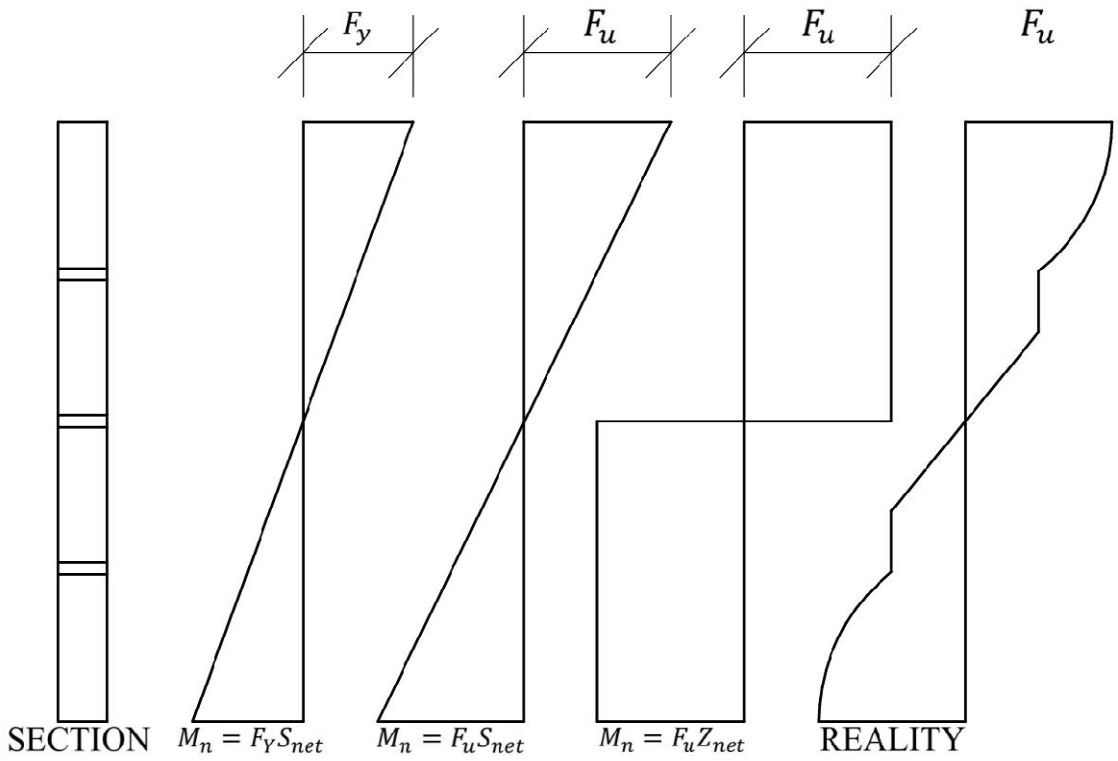

Figure 4: Flexural Rupture Equations and their Cross-Section Assumptions

1.3 Project Objectives

The primary objectives of this research are as follows:

- Perform research to discover if any experimental or analytical analysis has been conducted on any or all forms of the flexural rupture limit state equation.
- Analyze fiber-based models of various extended shear plate configurations to determine the true theoretical moment capacities of each.
- Compare the fiber-based results against the predicted capacities using the various AISC limit state equations.
- Develop conclusions and recommendations based on analytical and calculated results that obtain a more accurate procedure to find the flexural rupture capacity of a connecting element.

1.4 Scope of Work

This report will consider the analysis of twenty-four different extended shear plate configurations using combinations of variables such as bolt size, bolt number, bolt layout (spacing and edge distance), and bolt hole type (standard and oversized). The twenty-four different test configurations will consider extremes of each variable to understand how each may or may not affect the resulting flexural rupture capacities of the extended shear tab configurations. These configurations will then be analyzed against a series of equations suggested to find the flexural rupture capacity in accordance with the AISC manual (2017), as well as its earlier versions, to determine the accuracy of the recommended equation under various conditions.

The resulting data will finally be considered against a fiber model analysis to decide if the flexural rupture equation in question is accurate as it is for any of the tested scenarios, or if further experimental testing and analysis is required. The fiber analyses were performed using a idealized stress-strain curve assuming A36 steel only.

CHAPTER 2: LITERATURE REVIEW

2.1 AISC Steel Limit States Applicable for Connecting Elements Subject to Flexure

When transferring forces through connected members, certain construction scenarios may create an eccentric load path that develops flexure within the connecting elements and must consider multiple limit states as discussed in Chapter 1. The limit states for affected and connecting elements subject to flexure are yielding, lateral-torsional buckling, local buckling (Section J4.5 and Chapter F (AISC, 2016)), and flexural rupture (Part 10) in the AISC manual (AISC, 2016). Chapter F of the AISC Specification for Structural Steel Buildings (AISC, 2016), Section F11, shows that aside from flexural rupture, any rectangular-bar cross-sections need only consider the limit states of lateral-torsional buckling and flexural yielding. This report will be concentrating on the extended configuration of single-plate connections bent about the major axis and it will no longer discuss the limit states of lateral-torsional buckling and local buckling.

2.2 Flexural Rupture of Extended Configuration Single-Plate Connections

This report will discuss the flexural rupture limit state of extended configuration single-plate connections. The dimensional limitations that define extended configuration connections in Part 10-89 of the AISC Steel Construction Manual (AISC, 2016) are listed as follows:

1. The number of bolts, n, is not limited.
2. The distance from the weld line to the bolt line closest to the support, a, is not limited.
3. The use of holes must satisfy the AISC Specification Section J3.2 requirements.
4. The horizontal and vertical edge distances, l_{eh} and l_{ev}, must satisfy AISC Specification Table J3.4 requirements.

As seen above, the number of bolts as well as the distance of the closest bolt line to the weld line are not limited. This allows for a larger eccentricity to occur within the connection making flexural rupture a potential controlling limit state.

2.3 Experimental Studies Defining the Bending Strength of Steel Bracket and Splice Plates

The varying assumptions brought forth by each version of the flexural rupture limit state equation are inherently flawed as they assume stress distributions in the cross-section that cannot realistically be achieved. Few experimental studies have been conducted to investigate and analyze the real-world accuracy of the equations. No reports could be found to fully explain how each version came to be.

In 2008, Mohr and Murray setup an experiment to analyze each version of the flexural rupture limit state equation and compare the predicted strength values to experimental results. The current AISC Steel Construction Manual (AISC, 2016) references this experiment as the verification for the current flexural rupture limit state equation and its assumptions, as well as its minimum design checks.

2.3.1 Mohr and Murray

The experimentation done by Mohr and Murray (2008) was designed to compare the multiple AISC design limit equations and their predicted values to real world data gathered through the testing of beam splice plates subject to pure moment. The experimental setup shown in Figure 5 consisted of two W27x84, A992 steel, beams connected by two splice plates bolted through both beam webs. The total test setup was simply supported, and a spreader beam was used to induce two-point loads on either side of the splice plates in hopes of creating pure moment on the connection until the plates failed by flexural rupture.

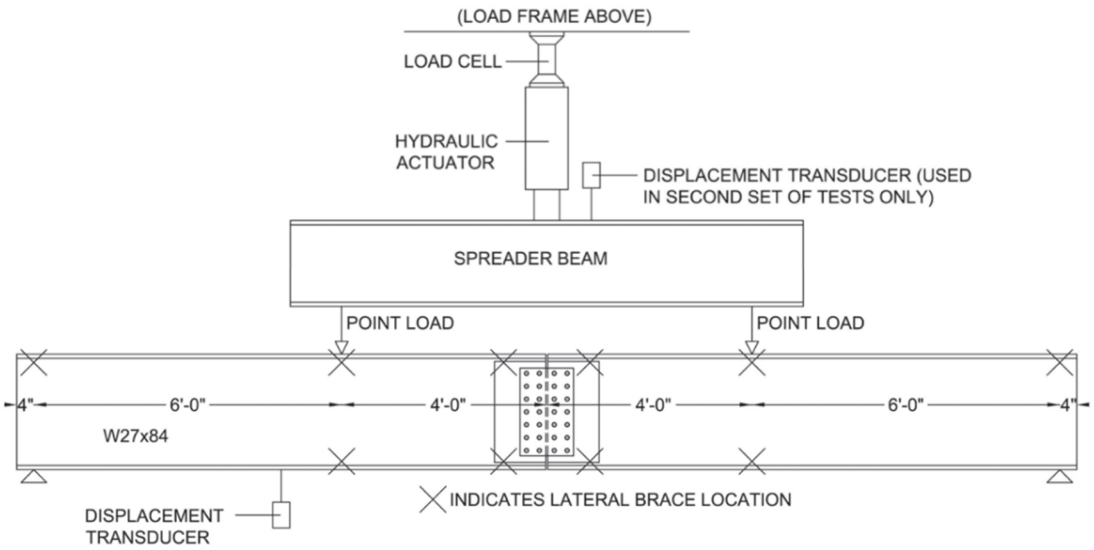

Figure 5: Schematic Diagram of Test Setup (Mohr and Murray, 2008)

Initial testing found that despite being laterally braced at ten locations along the beams, the compression flanges still showed rotational movement in relation to each other. Therefore, a channel was fitted over top of the flanges of both beams to restrict this movement. A large gap was also required between the splice plates to ensure the compression flanges did not touch when large deflections occurred. The plates also tended to move laterally towards or away from one another at the connection centerline, so a bolt, washers, and a snug-tight nut were added at the middle top of the plate and made to act as a stabilizer to restrict this movement. The basic bolt layout and geometry of the splice plates are shown in Figure 6.

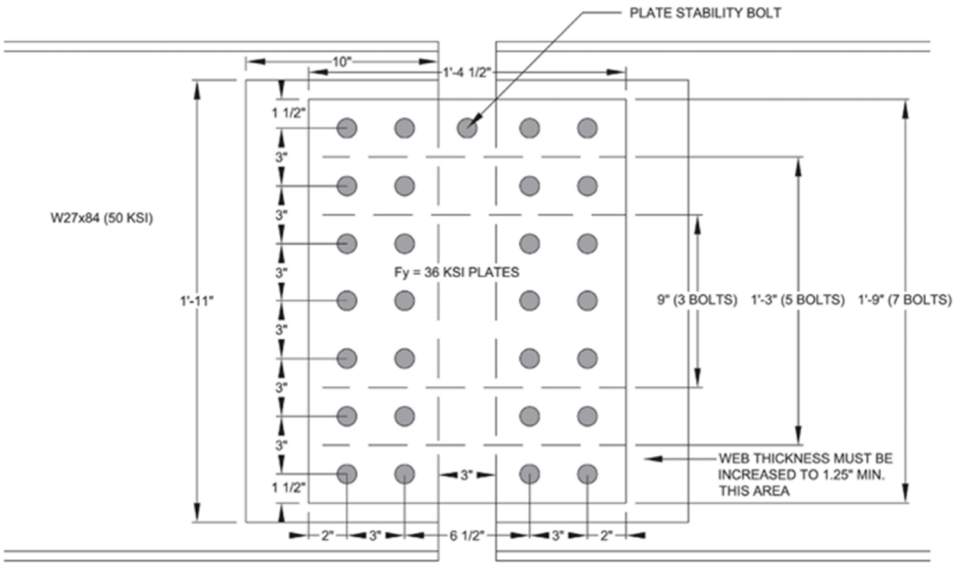

Figure 6: Splice Plate Geometry (Mohr and Murray, 2008)

Three larger steel plates (referred to as "Heats") were used to make the splice plate specimens. Heat 1 was a 3/8 inch thick sheet of A36 steel, Heat 2 was a 5/8 inch thick sheet of A36 steel, and Heat 3 was a 3/8 inch thick sheet of prefabricated steel supplied by the sponsor. All three materials were tested for tensile strength with results as shown in Table 1.

Table 1: Measured Splice Plate Material Properties (Mohr and Murray, 2008)

Table 1. Measured Splice Plate Material Properties			
Heat	F_y (ksi)	F_u (ksi)	Elongation
1	49.5	72.1	N/A
2	48.4	63.7	47%
3	71.8	88.1	N/A

The Heat 1 material was used to create plates using three different bolt configurations. The configurations made use of 3, 5, or 7 bolt rows, and all used ¾ inch diameter bolts. Each configuration was fabricated twice, resulting in a total of six plates using Heat 1 material.

Similar to Heat 1, the Heat 2 material was used to create plates using three different bolt configurations. These configurations again made use of 3, 5, or 7 bolt rows, but used 1 inch diameter bolts. Each configuration was fabricated twice, resulting in a total of six plates using Heat 2 material.

The Heat 3 material was used to create only one bolt configuration comprised of 5 bolt rows with 1 inch diameter bolts. This configuration was also fabricated twice to result in a total of two plates using the Heat 3 material.

The naming convention used for the test numbers can be read as number of bolt rows, bolt diameter, heat number, plate thickness, and A or B designating the first and second experiment using that configuration, respectively. Table 2 summarizes the test specimens and their chosen properties.

Table 2: Specimen Matrix (Mohr and Murray, 2008)

	Test No.	Bolt Rows (A90 Bolts)	Bolt Diameter (in.)	Measured Plate Thickness (in.)	Height (in.)	Width (in.)	Tightening Method
Heat 1	3-3/4-H1-3/8-A	3	¾	0.370	9	16.5	Impact Wrench
	3-3/4-H1-3/8-B	3	¾	0.370	9	16.5	Spud Wrench
	5-3/4-H1-3/8-A	5	¾	0.370	15	16.5	Impact Wrench
	5-3/4-H1-3/8-B	5	¾	0.370	15	16.5	Impact Wrench
	7-3/4-H1-3/8-A	7	¾	0.370	21	16.5	Impact Wrench
	7-3/4-H1-3/8-B	7	¾	0.370	21	16.5	Impact Wrench
Heat 2	3-1-H2-5/8-A	3	1	0.620	9	16.5	Impact Wrench
	3-1-H2-5/8-B	3	1	0.620	9	16.5	Impact Wrench
	3-1-H2-5/8-C	3	1	0.620	9	16.5	Impact Wrench
	5-1-H2-5/8-A	5	1	0.620	15	16.5	Impact Wrench
	5-1-H2-5/8-B	5	1	0.620	15	16.5	Impact Wrench
	5-1-H2-5/8-C	5	1	0.620	15	16.5	Impact Wrench
Heat 3	5-1-H3-3/8-A	5	1	0.381	15	16.5	Spud Wrench
	5-1-H3-3/8-B	5	1	0.381	15	16.5	Impact Wrench

Most of the tests in Table 2 resulted in a failure mode of flexural rupture. However, some tests resulted in deflections of over 8 inches before reaching flexural rupture. This deflection was considered excessive and these tests were terminated before flexural rupture could be achieved. It is important to note that although these tests were concluded before the flexural rupture limit state was reached, these connection configurations may still have failed by flexural rupture if these tests continued.

Table 3 shows the resulting yield and ultimate moments of each test as well as its failure mode.

Table 3: Test Results (Mohr and Murray, 2008)

	Test No.	No. of Bolt Rows	Observed First Yield Moment M_{ye} (kip-ft)	Maximum Applied Moment M_{ue} (kip-ft)	Failure Mode
Heat 1	3-3/4-H1-3/8-A	3	23	34.2	Flexural Rupture
	3-3/4-H1-3/8-B	3	22	31.5	Flexural Rupture
	5-3/4-H1-3/8-A	5	67	91.7	Flexural Rupture
	5-3/4-H1-3/8-B	5	70	88.8	Flexural Rupture
	7-3/4-H1-3/8-A	7	118	167.1	Flexural Rupture
	7-3/4-H1-3/8-B	7	122	175.4	Flexural Rupture
Heat 2	3-1-H2-5/8-A	3	39	48.3	Excessive Deflection
	3-1-H2-5/8-B	3	37	53.6	Excessive Deflection
	3-1-H2-5/8-C	3	35	51.5	Excessive Deflection
	5-1-H2-5/8-A	5	106	169.5	Flexural Rupture
	5-1-H2-5/8-B	5	107	134.4	Excessive Deflection
	5-1-H2-5/8-C	5	100	152.1	Flexural Rupture
Heat 3	5-1-H3-3/8-A	5	70	107.3	Excessive Deflection
	5-1-H3-3/8-B	5	84	117.8	Flexural Rupture

Figure 7 shows the measured deflection in relation to the applied moment for two of the tests, one from Heat 1 that failed due to flexural rupture and one from Heat 2 that failed due to excessive deflection. “The nonlinear response up to approximately 10 kip-ft is attributed to the movement at the bolt holes since the bolts were only snug tight. The experimental yield point is defined as the intersection of the elastic and strain hardening slopes of the curves, as shown in Figure 7. Also shown in the figure are the predicted plate yield moments for each test, $F_y S_{gross}$, using measured material properties” (Mohr and Murray, 2008).

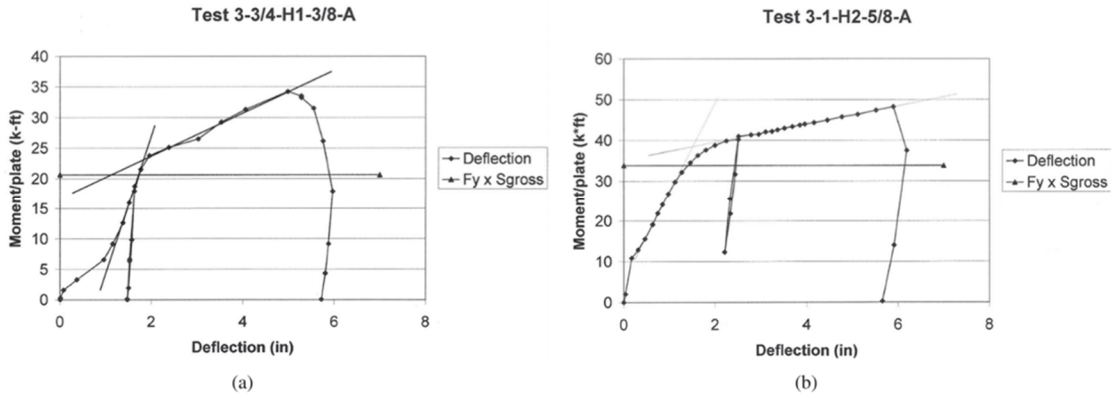

Figure 7: Representative Moment vs. Deflection Plots (Mohr and Murray, 2008)

Figure 7 shows the importance that stress-strain curve assumptions have on the actual flexural rupture capacity of a connection. As shown in

Table 4, if the outlying Test 5-1-H3-3/8-A is excluded, the mean ratio of the predicted first yield moment, calculated using the measured plate strengths, to the experimental first yield moment of all tests was 9% conservative.

Table 4: Comparison of Test Data with Predicted First Yield Moment Values (Mohr and Murray, 2008)

	Test No.	First Yield Moment M_{ye} (kip-ft)	F_y (ksi)	S_{gross} (in.^{3})	F_yS_{gross} (kip-ft)	$\frac{F_yS_{gross}}{M_{ye}}$
Heat 1	3-3/4-H1-3/8-A	23	49.5	5.00	20.6	0.89
	3-3/4-H1-3/8-B	22	49.5	5.00	20.6	0.93
	5-3/4-H1-3/8-A	67	49.5	13.88	57.3	0.85
	5-3/4-H1-3/8-B	70	49.5	13.88	57.3	0.82
	7-3/4-H1-3/8-A	118	49.5	27.20	112	0.95
	7-3/4-H1-3/8-B	122	49.5	27.20	112	0.92
Heat 2	3-1-H2-5/8-A	39	48.4	8.37	33.8	0.86
	3-1-H2-5/8-B	37		8.37	33.8	0.91
	3-1-H2-5/8-C	35	48.4	8.37	33.8	0.96
	5-1-H2-5/8-A	106	48.4	23.25	93.8	0.88
	5-1-H2-5/8-B	107	48.4	23.25	93.8	0.88
	5-1-H2-5/8-C	100	48.4	23.25	93.8	0.93
Heat 3	5-1-H3-3/8-A	70	71.8	14.29	85.5	1.22
	5-1-H3-3/8-B	84	71.8	14.29	85.5	1.02

Mohr and Murray (2008) calculated the predicted moments using all previous flexural rupture equations and compared them to the maximum applied experimental moment, M_{ue}.

These resulting moment capacities are shown in Table 5, as well as the ratios of predicted moments (using measured plate strengths shown in Table 1) to the maximum experimental moments. In Heat 1, the calculated moment capacities for $F_y Z_{gross}$ and $F_u Z_{net}$ differ by less than 5% with $F_y Z_{gross}$ resulting in the smallest calculated strength for each Heat 1 test. When compared to the maximum experimental moment capacity, this equation is found to be about 4% conservative. The majority of the Heat 2 tests (four of six) were concluded due to excessive deflection before flexural rupture could be reached. However, it is unknown if extended testing would have failed due to flexural rupture. The ratio of the minimum calculated strengths to maximum experimental strengths using $F_u Z_{net}/M_{ue}$, in Heat 2, show a conservative result of around 17%. Heat 3 had a split result between failing due to flexural rupture and the test being concluded due to excessive deflection. This heat, however, resulted in a ratio of minimum calculated strengths to maximum experimental strengths using $F_u Z_{net}/M_{ue}$, that resulted in being about 11% conservative.

For all tests, the mean ratio of the predicted controlling limit state (being the minimum of $F_y Z_{gross}$ and $F_u Z_{net}$) and the maximum experimental moment (M_{ue}) was found to be 0.89 with no value exceeding 1.0.

Table 5: Comparison of Test Data with Existing Design Models (Mohr and Murray, 2008)

	Test No.	M_{ue} (kip-ft)	F_y (ksi)	F_u (ksi)	S_{net} (in.^{3})	Z_{gross} (in.^{3})	Z_{net} (in.^{3})	Z'_{net} (in.^{3})	$\frac{F_u S_{net}}{M_{ue}}$	$\frac{F_y Z_{gross}}{M_{ue}}$	$\frac{F_u Z_{net}}{M_{ue}}$	$\frac{F_u Z'_{net}}{M_{ue}}$
Heat 1	3-3/4-H1-3/8-A	34.2	49.5	72.1	3.70	7.49	5.48	6.24	0.65	0.90	0.96	1.10
	3-3/4-H1-3/8-B	31.5	49.5	72.1	3.70	7.49	5.48	6.24	0.70	0.98	1.04	1.19
	5-3/4-H1-3/8-A	91.7	49.5	72.1	9.97	20.81	14.91	17.26	0.65	0.94	0.98	1.13
	5-3/4-H1-3/8-B	88.8	49.5	72.1	9.97	20.81	14.91	17.26	0.67	0.97	1.01	1.17
	7-3/4-H1-3/8-A	167.1	49.5	72.1	19.42	40.79	29.07	33.83	0.70	1.00	1.05	1.21
	7-3/4-H1-3/8-B	175.4	49.5	72.1	19.42	40.79	29.07	33.83	0.66	0.96	1.00	1.16
Heat 2	3-1-H2-5/8-A	48.3	48.4	63.7	5.58	12.56	8.17	9.68	0.61	1.05	0.90	1.06
	3-1-H2-5/8-B	53.6	48.4	63.7	5.58	12.56	8.17	9.68	0.55	0.95	0.89	0.96
	3-1-H2-5/8-C	51.5	48.4	63.7	5.58	12.56	8.17	9.68	0.57	0.98	0.84	1.00
	5-1-H2-5/8-A	169.5	48.4	63.7	14.88	34.88	22.12	26.83	0.47	0.83	0.69	0.84
	5-1-H2-5/8-B	134.4	48.4	63.7	14.88	34.88	22.12	26.83	0.59	1.05	0.87	1.06
	5-1-H2-5/8-C	152.1	48.4	63.7	14.88	34.88	22.12	26.83	0.52	0.93	0.77	0.94
Heat 3	5-1-H3-3/8-A	107.3	71.8	88.1	9.14	21.43	13.60	16.49	0.63	1.19	0.93	1.13
	5-1-H3-3/8-B	117.8	71.8	88.1	9.14	21.43	13.60	16.49	0.57	1.09	0.85	1.03

Taking these ratios into account, Mohr and Murray (2008) suggested a new design model that assumes the compression area bolt holes can be neglected entirely while calculating the net plastic section modulus. Locating the plastic neutral axis by setting the area of the plate in tension equal to the area in compression, this new definition of the net plastic section modulus was defined as shown in Equation 2-1.

$$\boldsymbol{Z'_{net} = \Sigma |A_i d_i|} \qquad \textbf{Equation (2 - 1)}$$

Where:

A_i : area of plate section i

d_i : distance from center of section i to plastic neutral axis, as shown in Figure 8.

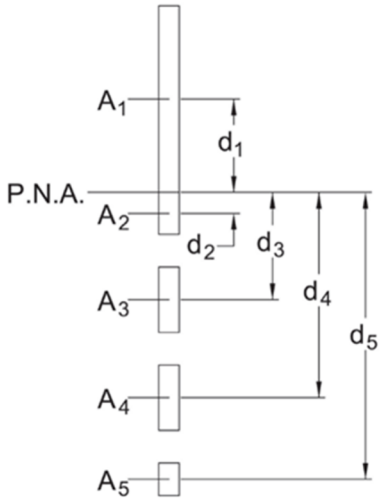

Figure 8: Terms used in calculation of Z'_{net} (Mohr and Murray, 2008)

This alternative design equation resulted in predicted moment ratios very close to those in the F_yZ_{gross} equation, however, were less conservative than the resulting ratios from the F_uZ_{net} equation, with some results over 1.0. "From the results of the 14 tests, the minimum of the predicted moments F_yZ_{gross} and F_uZ_{net}, or F_yZ_{gross} and $F_uZ'_{net}$, matches the controlling experimental failure mode and generally provides an accurate prediction of the maximum experimental moment. However, the use of $F_uZ'_{net}$ resulted in unconservative predictions for all of the Heat 1 tests" (Mohr and Murray, 2008).

2.4 Conclusions of Mohr and Murray Analysis and Verification of Current Design Models

A final comparison of available LRFD moment strengths was created by Mohr and Murray (2008) to show the difference in calculated values between the F_yZ_{gross} and F_uZ_{net} equations. As seen in Table 6, the controlling limit state is flexural rupture, F_uZ_{net}, for all connection configurations and steel types listed. With this comparison table and the experimental analysis results, the authors concluded that the flexural rupture equations used prior to the 13th Edition AISC Steel Construction Manual were excessively conservative and that "available moment strength in LRFD, ΦM_n, can safely be calculated as the minimum of $0.9F_yZ_{gross}$ and

$0.75F_uZ_{net}$, or in ASD as the minimum of $F_yZ_{gross}/1.67$ and $F_uZ_{net}/2.0$, which are the current AISC Manual design models" (Mohr and Murray, 2008).

Table 6: Comparison of Available Moment Strengths (Mohr and Murray, 2008)

No. of Bolts	Bolt Diameter (in.)	Nominal Moment Strength			
		F_y = 36 ksi	F_u = 58 ksi	F_y = 50 ksi	F_u = 65 ksi
		$0.9F_yZ_{gross}$ (kip-ft)	$0.75F_uZ_{net}$ (kip-ft)	$0.9F_yZ_{gross}$ (kip-ft)	$0.75F_uZ_{net}$ (kip-ft)
2	¾	24.3	23.1	33.8	25.9
	⅞	24.3	21.8	33.8	24.4
	1	24.3	20.4	33.8	22.9
3	¾	54.7	53.7	75.9	60.2
	⅞	54.7	50.8	75.9	56.9
	1	54.7	47.8	75.9	53.6
4	¾	97.2	92.4	135	103
	⅞	97.2	87.0	135	94.5
	1	97.2	81.6	135	91.4
5	¾	151	146	210	163
	⅞	151	137	210	154
	1	151	129	210	145
6	¾	218	208	303	233
	⅞	218	195	303	219
	1	218	183	303	205
7	¾	297	284	413	319
	⅞	297	268	413	300
	1	297	251	413	282
8	¾	388	369	540	414
	⅞	388	348	540	390
	1	388	326	540	365
9	¾	492	469	683	526
	⅞	492	442	683	495
	1	492	414	683	464
10	¾	607	577	843	647
	⅞	607	543	843	609
	1	607	509	843	571

CHAPTER 3: TESTING METHODOLOGY

3.1 Introduction

As seen in the experimental analysis done by Mohr and Murray (2008), the assumptions put forth in the stress-strain curve and the behavior of the section under stress can vastly change the predicted flexural rupture strength capacity of a given connection configuration. The use of a fiber-based model will give an accurate depiction of the stresses within a section, and how those section properties actually behave under those stresses. This is accomplished by separating the connection component cross-section into many layers, called fibers, from top to bottom. The stresses in each fiber are accounted for to determine the actual maximum moment capacity of the cross-section, which will be compared to the predictive flexural rupture equations to determine the accuracy of each.

3.1.1 Fiber-Based Model Test Matrix

Table 7 shows the fiber-based model test matrix that was formed by determining specific variables to create extreme connection scenarios in which flexural rupture would need to be addressed. These variables are defined as follows:

- n : Number of Bolts
- d_b : Bolt Diameter
- L_e : Bolt Center to Edge Distance
- s : Bolt Center to Center Spacing
- d_h : Bolt Hole Diameter

The test matrix consists of connection configurations containing 3, 4, and 5 bolt rows. Each set of bolt rows was analyzed once considering standard bolt hole diameters, and then again considering oversized bolt hole diameters. The bolt diameters chosen were 7/8 inch and 1 inch,

and the spacing conditions chosen included both AISC preferred minimums as well as AISC absolute minimums, as discussed in Section J3 of the AISC specification (AISC, 2016). The test runs and their chosen variables are as shown in Table 7 below.

Table 7: Fiber-Based Model Test Matrix

TEST NUMBER	TEST NAME	NUMBER OF BOLTS n	BOLT DIAMETER d_b [in]	BOLT CENTER TO CENTER SPACING s [in]	BOLT CENTER TO EDGE DISTANCE L_e [in]
1	3A	3	7/8	3	1 1/8
2	3B	3	7/8	3	1 1/2
3	3C	3	1	3	1 1/4
4	3D	3	1	3	1 1/2
5	4A	4	7/8	3	1 1/8
6	4B	4	7/8	3	1 1/2
7	4C	4	1	3	1 1/4
8	4D	4	1	3	1 1/2
9	5A	5	7/8	3	1 1/8
10	5B	5	7/8	3	1 1/2
11	5C	5	1	3	1 1/4
12	5D	5	1	3	1 1/2
13	3A OVS	3	7/8	2 1/3	1 3/16
14	3B OVS	3	7/8	2 5/8	1 3/16
15	3C OVS	3	1	2 2/3	1 3/8
16	3D OVS	3	1	3	1 3/8
17	4A OVS	4	7/8	2 1/3	1 3/16
18	4B OVS	4	7/8	2 5/8	1 3/16
19	4C OVS	4	1	2 2/3	1 3/8
20	4D OVS	4	1	3	1 3/8
21	5A OVS	5	7/8	2 1/3	1 3/16
22	5B OVS	5	7/8	2 5/8	1 3/16
23	5C OVS	5	1	2 2/3	1 3/8
24	5D OVS	5	1	3	1 3/8

3.2 Plate Flexural Rupture Predictions

For all analytical cases from the test matrix described in Section 3.1, flexural rupture capacities were compared against each of the three historical AISC Steel Construction Manual

predictive equations. Each of the three equations assume a different stress distribution in the net cross-section. A typical graph showing the different assumed stresses in comparison to the actual behavior of the cross-section as discovered through the fiber-based analysis is shown in Figure 9.

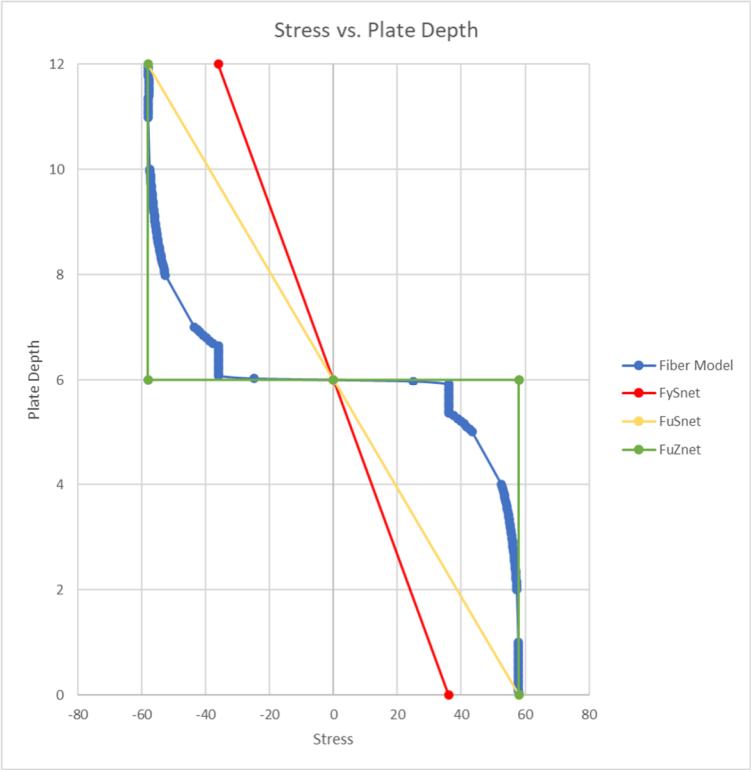

Figure 9: Average Stress vs. Plate Depth Graph (Test 4B)

As seen in Figure 9, Equations (1-1) and (1-2) assume a linear relationship between the distance from the neutral axis and the stress at any point in the plate. Equations (1-1) and (1-2) also assume that the ends of the plate reach the plate yield stress and ultimate stress, respectively. Equation (1-3), on the other hand, assumes both sides of the plate (tension and compression sides) reach the plate ultimate stress within the entire net cross-section. A more accurate behavior of the cross-section can be seen from the fiber model as behaving differently than all of these predictive equations.

These equations assume either yield stress or ultimate stress as the value chosen to determine the maximum flexural rupture capacity. However, Equation 1-3 uses the plastic section modulus, while the previous equations use the elastic section modulus. As previously discussed, the plastic section modulus assumes the entire cross-section is at the ultimate stress, which is unrealistic. AISC Section 15-4 (AISC, 2016) discusses the calculation of the plastic section modulus for elements in flexure with two equations, one for an odd number of bolt rows and one for an even number of bolt rows. These equations both make use of a variable d'_h, which is diameter of the bolt hole, plus a given tolerance of 1/16 inch (used in steel design equations for all fracture limit states). These equations also specify that the vertical edge distance is assumed to be half the spacing. Since the fiber-based model was set up to account for the actual size of the bolt holes and excluded the additional 1/16 inch and because this research investigated cases in which the edge distance was not ½ of the bolt spacing, these equations were not used to calculate the plastic section modulus. Instead, the plastic section modulus was calculated as shown in Equation (3-1), with y_{bar} being calculated by taking the sum of the distances from each tension fiber center to the center of the plate multiplied by each fiber area, and divided by the area of fibers in tension, or half of the plate (y_{bar} for the tension side is the same for the compression side due to symmetry):

$$\boldsymbol{Z_{net} = \frac{A}{2}(2y_{bar})} \qquad \textbf{Equation (3 - 1)}$$

This equation for the plastic section modulus accounted for the actual size of the bolt holes and did not consider the 1/16 inch tolerance used in the AISC equations.

3.3 Stress-Strain Curve and Plate Section Assumptions

The fiber-based model used in this report assumed an idealized, yet realistic stress-strain curve which was developed using research by Alvarez Rodilla (2020). His Master's Thesis, titled

"Experimental and Analytical Studies of Steel Members Subjected to Concentrated Loads with an Emphasis on Eccentric Stiffiner Design" (Alvarez Rodilla, 2020) experimentally tested steel members of type A992 under concentrated loads, with and without stiffeners. The relationship between stress and strain discovered in this testing was used to create the fiber-based model assumptions for the behavior of steel type A36.

The strain at the beginning of the yield plateau region is found to be the yield stress of the steel divided by the elastic modulus of 29000 ksi. From the experimental results of the A992 steel, the difference in strain from the beginning to the end of the yield plateau region is found to be about 0.0203 in/in. This difference is added to the strain value at the beginning of the yield palteau found for A36 steel, to find the point at the beginning of the strain hardening curve.

For each following point along the strain hardening region of the A992 experimental results, the incremental change in stress, divided by the difference between the ultimate and yield stresses was found. This value multiplied by the difference between the ultimate and yield stresses for A36 steel resulted in the incremental change in stress associated with A36 steel. This process was used for each point along the A992 strain hardening curve in order to discover the corresponding values of stress in the A36 curve. Assuming that the incremental change in strain for each point of the A992 curve can be directly related to the A36 curve, the strain values could be calculated as the stress divided by the elastic modulus, plus the incremental change in strain found in the A992 curve.

The curves created from this analysis are shown in Figure 10 and the fifth order equations computed for each curve were found using Microsoft Excel. The equation for the A36 steel curve was used in the fiber-based model as the assumption for the stress-strain behavior within the strain hardening region.

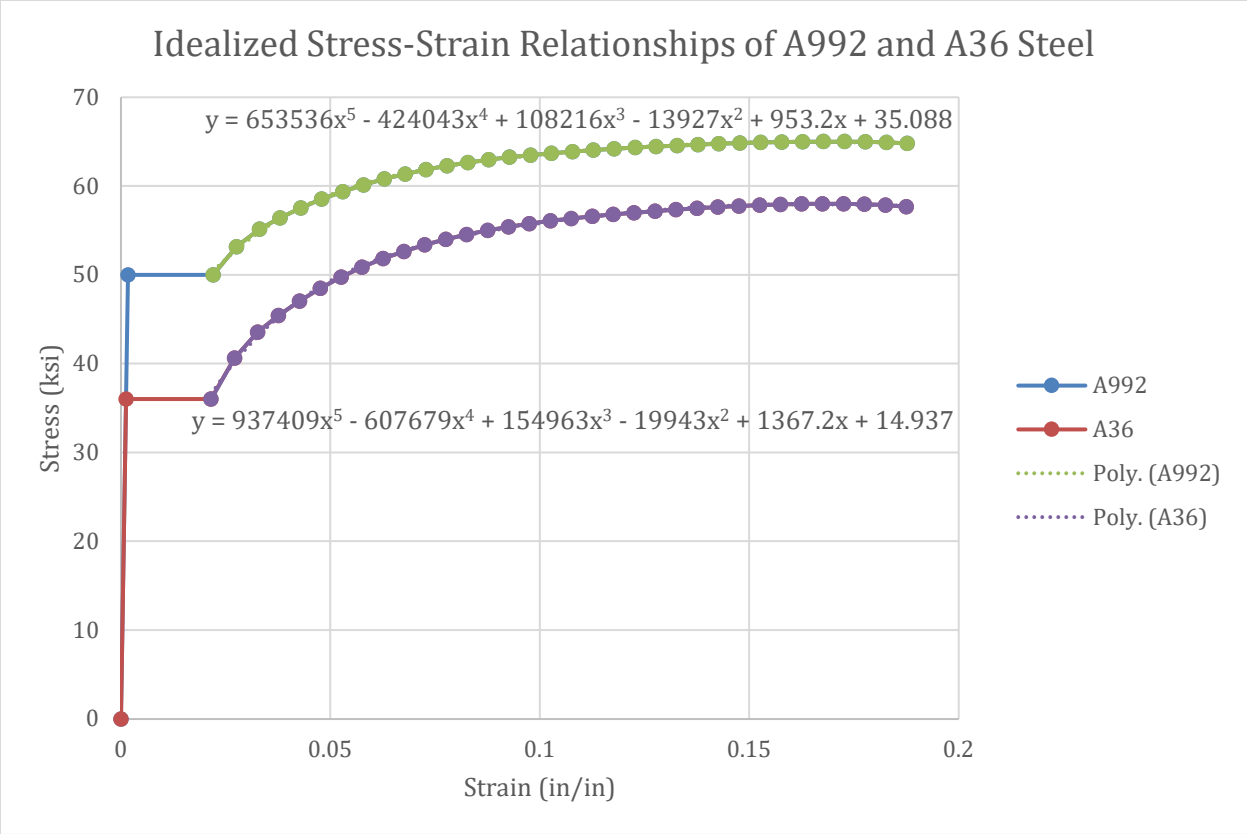

Figure 10: Idealized Stress-Strain Relationships of A992 and A36 Steel

3.4 Fiber-Based Model Analysis Procedure

After the test matrix was finalized and all variables were chosen, analytical testing could begin by creating a fiber-based model. As shown in Figure 11, for each set of bolt rows, 20 "edge" fibers and 40 "spacing" fibers (between bolt holes) were chosen for analysis. The edge fibers spanned from the edge of the plate to the edge of the first bolt hole, and the spacing fibers spanned from the edge of one bolt hole to the next. The center of each fiber was found along with its distance from the center of the plate configuration, and its area was found based on the plate thickness of ½ inch.

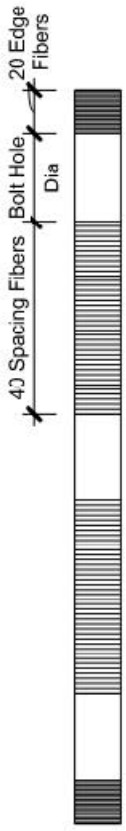

Figure 11: Discretization of plate cross-section into fibers

In order for flexural rupture to occur, it is assumed that the edge of the A36 steel plate has reached a stress equal to its ultimate stress of 58 ksi. Therefore, the very top and bottom fibers are assumed to have reached the stress of positive and negative 58 ksi, respectively. The force in all fibers is calculated as the stress multiplied by the fiber area. This force, multiplied by the distance from the center of the plate to the center of the fibers, results in a moment value that contributes to the overall moment in the plate. This process is completed for each fiber in the model, and a summation is done to calculate the final moment capacity of the plate at the point of flexural rupture.

Elastic behavior occurs up until the onset of strain hardening. This means that the stress can be defined as the elastic modulus of steel (29000ksi) multiplied by the strain at any given point where the strain is lesser than the yield strain. When the strain is larger than the yield

strain, but less than the strain at strain hardening, the stress is equal to the yield stress. After this point, where the strain is larger than that at strain hardening, plastic behavior occurs and the curve equation discussed earlier is the defining relationship between stress and strain until flexural rupture is reached. However, strain can also be defined as the distance from the center of the plate to the center of the fiber multiplied by a curvature value. The curvature values are incrementally increased to solve for the strains, forces, and moments in each fiber as described above. The resulting moments and the corresponding curvature values can be shown in the figure below, as well as the maximum flexural rupture moment capacity as calculated in each predictive equation. Although the assumed linear behavior of the moment curvature graph seems to shift starting at F_yS_{net}, there is still more moment capacity before the curve reached F_uS_{net}. It can also be seen that the F_uZ_{net} equation lies outside the moment curvature graph due to its assumption of the entire cross-section reaching F_u. The last point in this plot is the most significant for this research as it defines the moment capacity at which the most exterior fibers of the plate configuration, those furthest from the neutral axis, have reached the ultimate stress.

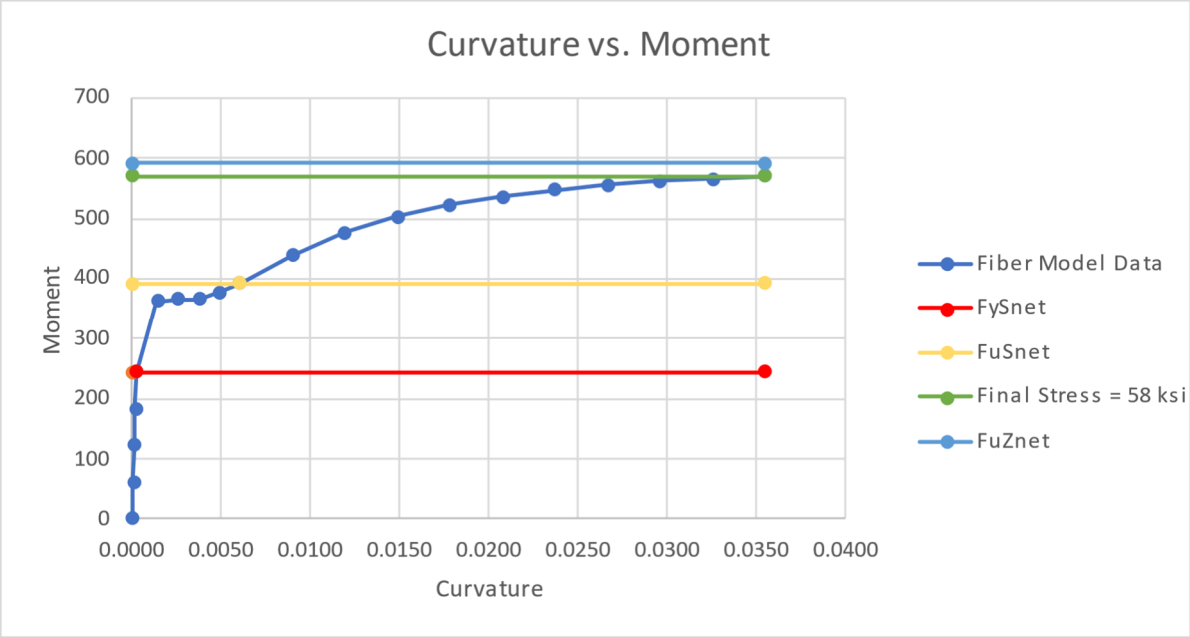

Figure 12: Curvature vs. Moment Graph (Test 4A)

CHAPTER 4: TESTING RESULTS

4.1 Introduction

After the development and analysis of the fiber-based models, the resulting data was compiled and compared to the calculated predictive equations previously defined in the AISC Steel Construction Manual (AISC, 2017). The results for each of the twenty-four tests determined the validity of each of the equation assumptions by comparing the final moment capacities to the calculated moment capacities to find a percentage difference between the fiber-based model and each equation.

4.2 Fiber-Based Model Results and Comparison to AISC Limit States

Table 8 compares moment capacities of the fiber-based models to those of the first flexural rupture equation historically put forth by the AISC Steel Construction Manual, Equation (1-1). As shown below, this equation predicts significantly lower moment capacities in comparison to the maximum moments obtained in the fiber-based models. The equation was drastically conservative for all 3 bolt rows configurations as the predicted moment capacity was calculated to be less than 30% of the fiber-based model moment capacity. The average percentage of all the calculated values was only 38%, with a median of less than 43%.

Table 8: Fiber-Based Model and Equation (1-1) Comparison

TEST MATRIX		RESULTS		
TEST NO.	TEST NAME	Equation (1-1) $M_n = F_y S_{net}$	Fiber Model M	% of Fiber Model
		[kip-in]	[kip-in]	
1	3A	88.26	309.33	28.53%
2	3B	108.82	400.82	27.15%
3	3C	84.93	304.73	27.87%
4	3D	99.36	366.76	27.09%
5	4A	243.63	569.69	42.77%
6	4B	304.61	693.26	43.94%
7	4C	236.66	547.17	43.25%
8	4D	278.70	630.64	44.19%
9	5A	394.98	935.87	42.20%
10	5B	471.67	1090.58	43.25%
11	5C	377.77	889.06	42.49%
12	5D	430.57	993.30	43.35%
13	3A OVS	53.75	199.15	26.99%
14	3B OVS	66.14	240.76	27.47%
15	3C OVS	69.61	259.77	26.80%
16	3D OVS	85.59	319.36	26.80%
17	4A OVS	151.08	338.36	44.65%
18	4B OVS	185.16	423.10	43.76%
19	4C OVS	195.69	438.59	44.62%
20	4D OVS	239.78	558.09	42.97%
21	5A OVS	231.86	531.86	43.59%
22	5B OVS	291.13	678.97	42.88%
23	5C OVS	299.35	687.84	43.52%
24	5D OVS	376.06	894.73	42.03%

Table 9 compares the moment capacities of the fiber-based model to the second flexural rupture equation put forth by the AISC Steel Construction Manual. This table also shows that all test runs with 3 bolt rows were the most conservative with none being more than 46% of the fiber-based model calculated moment capacities. The rest of the tests were all under 72% of the fiber-based model values. The overall average of Equation (1-2) in comparison with the fiber-based model was only 61% with a median of 69%.

Table 9: Fiber-Based Model and Equation (1-2) Comparison

TEST MATRIX		RESULTS		
TEST NO.	TEST NAME	Equation 1-2 $M_n = F_u S_{net}$	Fiber Model M	% of Fiber Model
		[kip-in]	[kip-in]	
1	3A	142.20	309.33	45.97%
2	3B	175.32	400.82	43.74%
3	3C	136.83	304.73	44.90%
4	3D	160.08	366.76	43.65%
5	4A	392.52	569.69	68.90%
6	4B	490.76	693.26	70.79%
7	4C	381.29	547.17	69.68%
8	4D	449.01	630.64	71.20%
9	5A	636.36	935.87	68.00%
10	5B	759.91	1090.58	69.68%
11	5C	608.63	889.06	68.46%
12	5D	693.70	993.30	69.84%
13	3A OVS	86.60	199.15	43.49%
14	3B OVS	106.56	240.76	44.26%
15	3C OVS	112.14	259.77	43.17%
16	3D OVS	137.89	319.36	43.18%
17	4A OVS	243.40	338.36	71.94%
18	4B OVS	298.31	423.10	70.50%
19	4C OVS	315.28	438.59	71.88%
20	4D OVS	386.32	558.09	69.22%
21	5A OVS	373.55	531.86	70.24%
22	5B OVS	469.04	678.97	69.08%
23	5C OVS	482.28	687.84	70.12%
24	5D OVS	605.87	894.73	67.72%

Table 10 compares the fiber-based model moment capacities with the final and current flexural rupture equation put forth by the AISC Steel Construction Manual. Equation (1-3) did not result in conservative values among the 3 bolt row configurations only as Equations (1-1) and (1-2) did. Instead, all of the Equation (1-3) results were above the values found from the fiber-based model analysis with both an average and median of almost 104%. The smallest overage in these comparisons was Test Number 20 being just 1% above the fiber-based model

results. Overall, the calculated results from Equation (1-3) were much more aligned with the fiber-based model analysis. Even though it was realized that in this research that Equation 1-3 assumes an unrealistic stress-strain curve, with the entire cross-section reaching the ultimate stress simultaneously, the differences between the moment capacity from the fiber model is small, even in extreme analytical test scenarios. This is primarily because the fibers that are farthest from the neutral axis, which reach F_u, contribute the most to the corresponding moment capacity.

Table 10: Fiber-Based Model and Equation (1-3) Comparison

TEST MATRIX		RESULTS		
TEST NO.	TEST NAME	Equation 1-3 $M_n = F_u Z_{net}$	Fiber Model M	% of Fiber Model
		[kip-in]	[kip-in]	
1	3A	323.60	309.33	**104.61%**
2	3B	417.75	400.82	**104.23%**
3	3C	318.64	304.73	**104.56%**
4	3D	382.32	366.76	**104.24%**
5	4A	590.97	569.69	**103.73%**
6	4B	717.75	693.26	**103.53%**
7	4C	567.06	547.17	**103.64%**
8	4D	652.50	630.64	**103.47%**
9	5A	976.10	935.87	**104.30%**
10	5B	1135.50	1090.58	**104.12%**
11	5C	927.64	889.06	**104.34%**
12	5D	1034.82	993.30	**104.18%**
13	3A OVS	207.54	199.15	**104.21%**
14	3B OVS	251.45	240.76	**104.44%**
15	3C OVS	269.10	259.77	**103.59%**
16	3D OVS	326.11	319.36	**102.12%**
17	4A OVS	349.64	338.36	**103.33%**
18	4B OVS	438.05	423.10	**103.53%**
19	4C OVS	451.21	438.59	**102.88%**
20	4D OVS	565.82	558.09	**101.39%**
21	5A OVS	554.33	531.86	**104.22%**
22	5B OVS	708.20	678.97	**104.30%**
23	5C OVS	713.77	687.84	**103.77%**
24	5D OVS	913.36	894.73	**102.08%**

CHAPTER 5: CONCLUSION AND RECOMMENDATIONS

5.1 Conclusions

- The current flexural rupture equation does a reasonable job in predicting the flexural moment capacity of a given plate configuration. In all cases, the current equation overpredicts the moment capacity by less than 5%. In using LRFD, there is a resistance factor of 0.75 when utilizing the equation. Therefore, one can make an argument that the equation can be utilized in design with minimal concerns.
- The previously used Equations (1-1) and (1-2) were extremely conservative, with moment capacity predictions averaging 38% and 61% of the fiber-based model results, respectively.

5.2 Recommendations

Considering that the current AISC flexural rupture equation predicts a moment capacity that is within 5% of the fiber-based model analytical results, and also considering a safety factor of 2 when using ASD and a resistance factor of 0.75 when using LRFD, the current flexural rupture limit state is acceptable. No changes are recommended. Since this research attempted to reach extremes for bolt spacing, edge distance, hole type, etc., no recommendations for further analytical studies are provided.

REFERENCES

AISC. (1989). *Allowable Stress Design Manual of Steel Construction.* (9th, Ed.) Chicago, IL: American Institute of Steel Construction.

AISC. (2001). *LRFD Manual of Steel Construction* (3rd ed.). Chicago, IL: American Institute of Steel Construction.

AISC. (2005). *Manual of Steel Construction* (13th ed.). Chicago, IL: American Institute of Steel Construction.

AISC. (2016). *Steel Construction Manual* (15th ed.). Chicago, IL: American Institute of Steel Construction.

AISC. (2017). *Specification for Structural Steel Buildings.* Chicago, IL: American Institute of Steel Construction.

Alvarez Rodilla, J. (2020). *Experimental and Analytical Studies of Steel Members Subjected to Concentrated Loads with an Emphasis on Eccentric Stiffiner Design.* Master's Thesis, Lawrence Technological University, Southfield, MI.

Mohr and Murray. (2008). *Bending Strength of Steel Bracket and Splice Plates.* American Institute of Steel Construction.

Stress-Strain Curve. (n.d.). What's Insight. Retrieved March 12, 2023 from https://whatsinsight.org/elastic-modulus-predicting-material-deformation-and-failure/

APPENDIX A: EXAMPLE CALCULATIONS

Example Moment Capacity Equations for Test Number 3A:

Variables:

F_y = 36 ksi, Fu = 58 ksi, d_b = 7/8 in, L_e = 1 1/8 in, d_h = 15/16 in, L = 8.25 in, L_c = 0.656 in, S_c = 2 1/16 in, e_{sh} = 0.21517, A=2.719 in^2, A_{edge} = 0.328125 in^2, A_{space} = 1.03125 in^2, y_{bar} = 4.12 in^2, S = 3 in, t = ½ in, n = 3

Calculations of S_{net} and Z_{net}:

$$S_{net} = \frac{I}{y_{bar}} = 2.45\ in^2$$

$$Z_{net} = \frac{A}{2}(2y_{bar}) = 5.58\ in^2$$

Calculations of Moment Capacities for Flexural Rupture Equations:

$$M_n = F_y S_{net} = 36ksi(2.45in^2) = 88.26 \text{ kip-in}$$

$$M_n = F_u S_{net} = 58ksi(2.45in^2) = 142.20 \text{ kip-in}$$

$$M_n = F_u Z_{net} = 58ksi(5.58in^2) = 323.60 \text{ kip-in}$$

Moment Curvature and Stress vs Plate Depth Graphs:

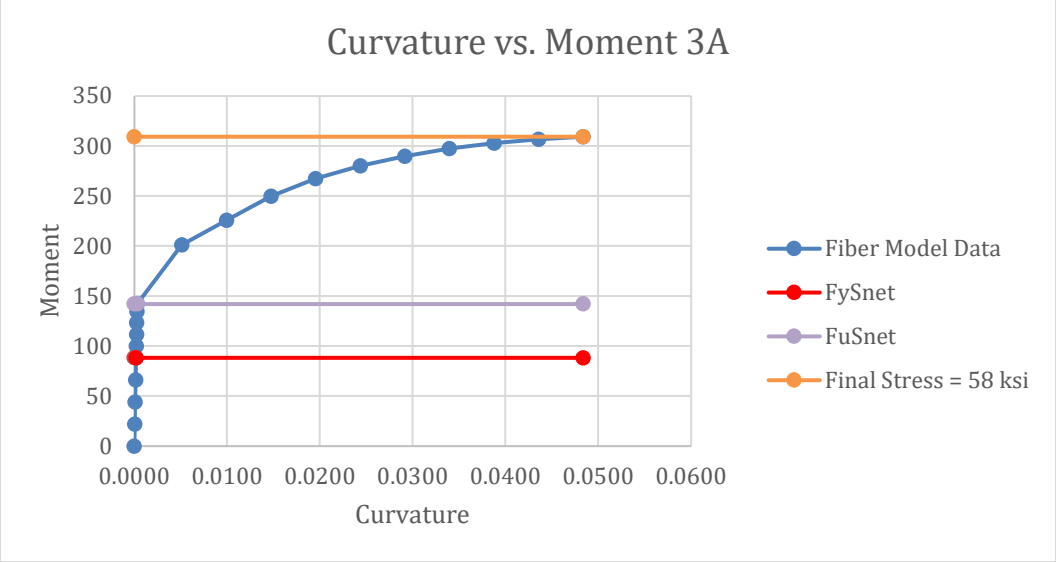

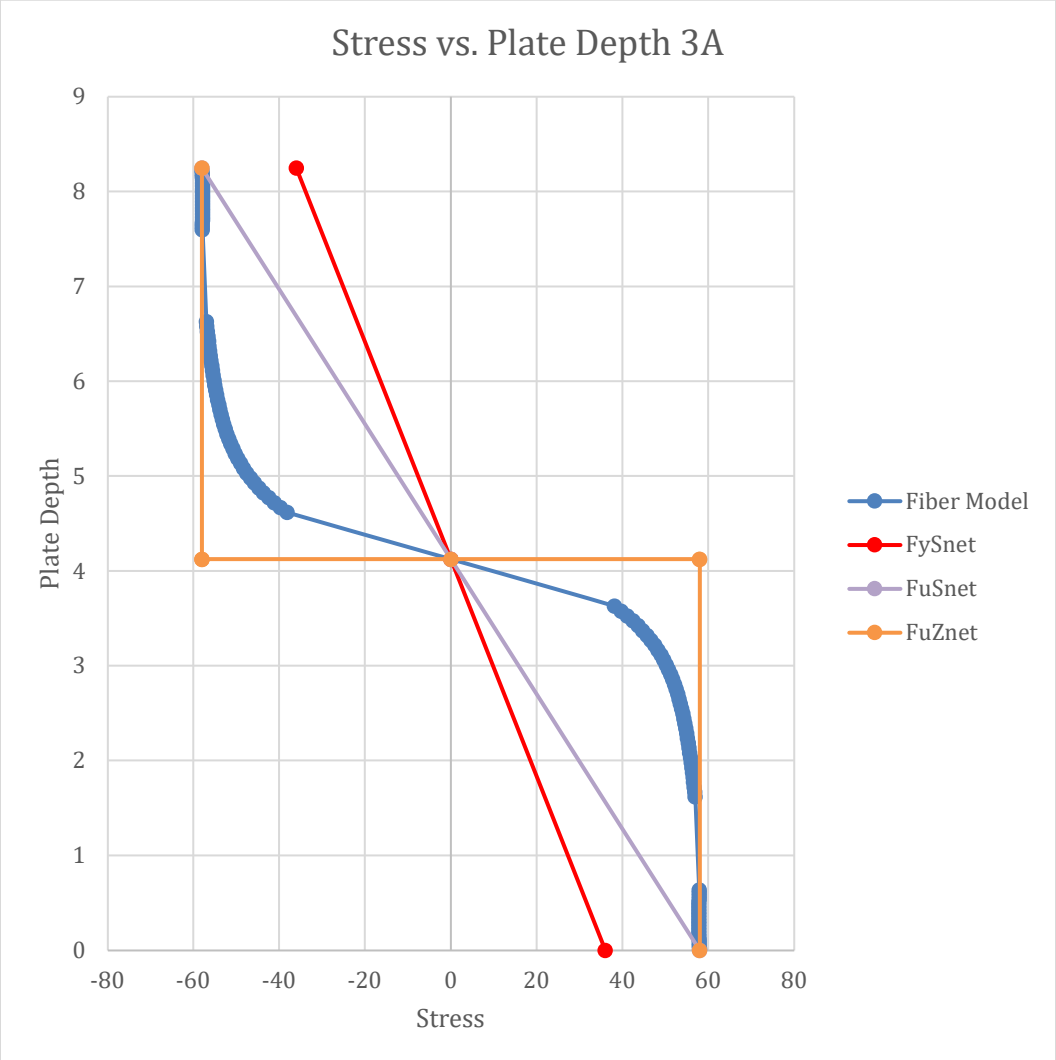

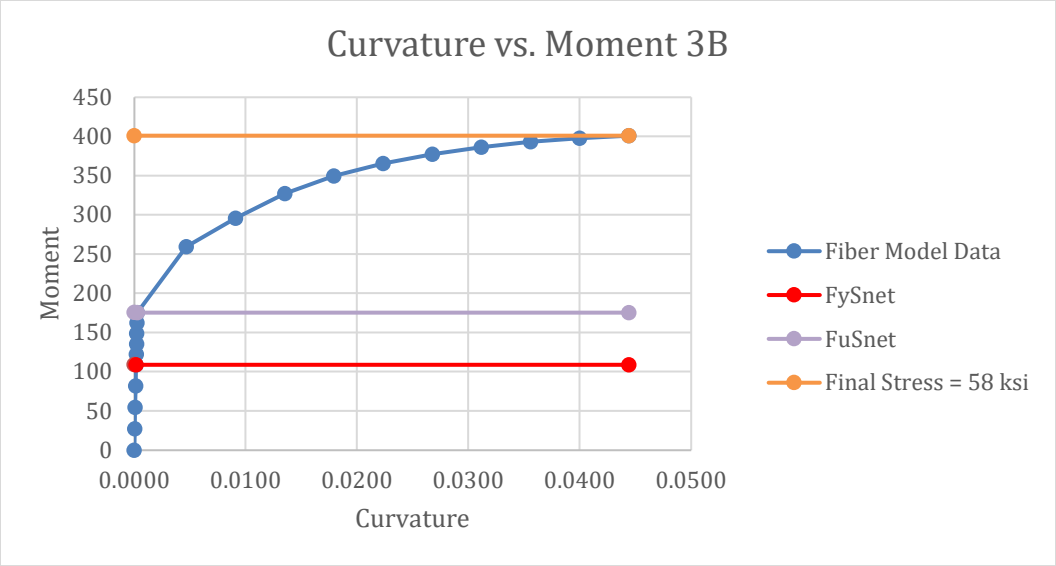
Curvature vs. Moment 3B
Moment
450
400
350
300
250
200
150
100
50
0
0.0000
0.0100
0.0200
0.0300
0.0400
0.0500
Curvature
Fiber Model Data
FySnet
FuSnet
Final Stress = 58 ksi

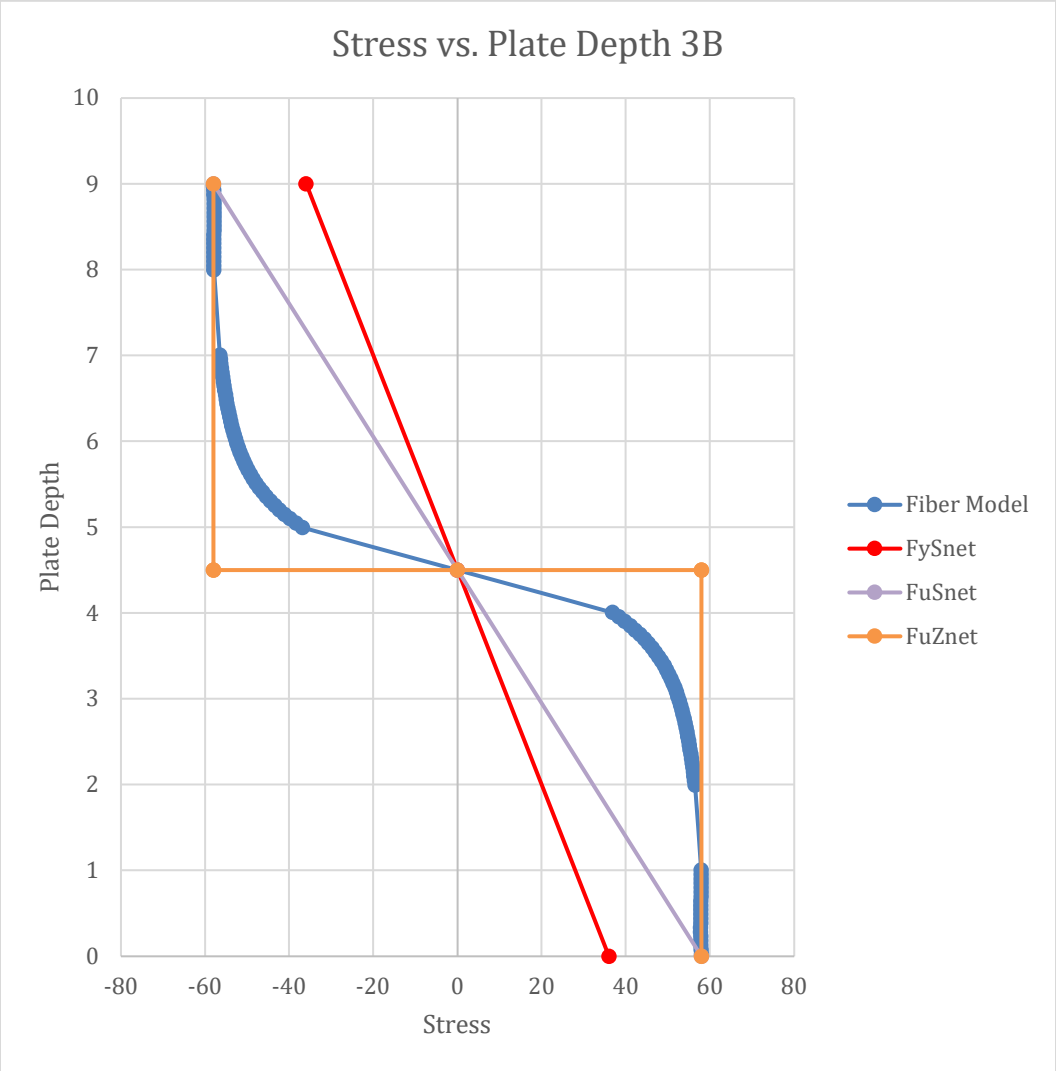
Stress vs. Plate Depth 3B
Plate Depth
10
9
8
7
6
5
4
3
2
1
0
-80
-60
-40
-20
0
20
40
60
80
Stress
Fiber Model
FySnet
FuSnet
FuZnet

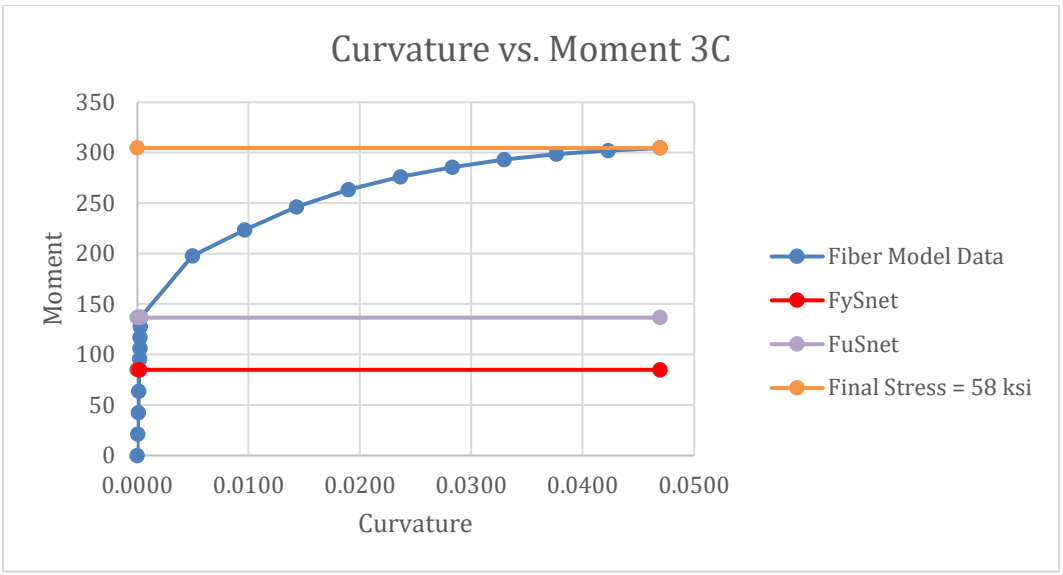
Curvature vs. Moment 3C
Moment
350
300
250
200
150
100
50
0
0.0000
0.0100
0.0200
0.0300
0.0400
0.0500
Curvature
Fiber Model Data
FySnet
FuSnet
Final Stress = 58 ksi

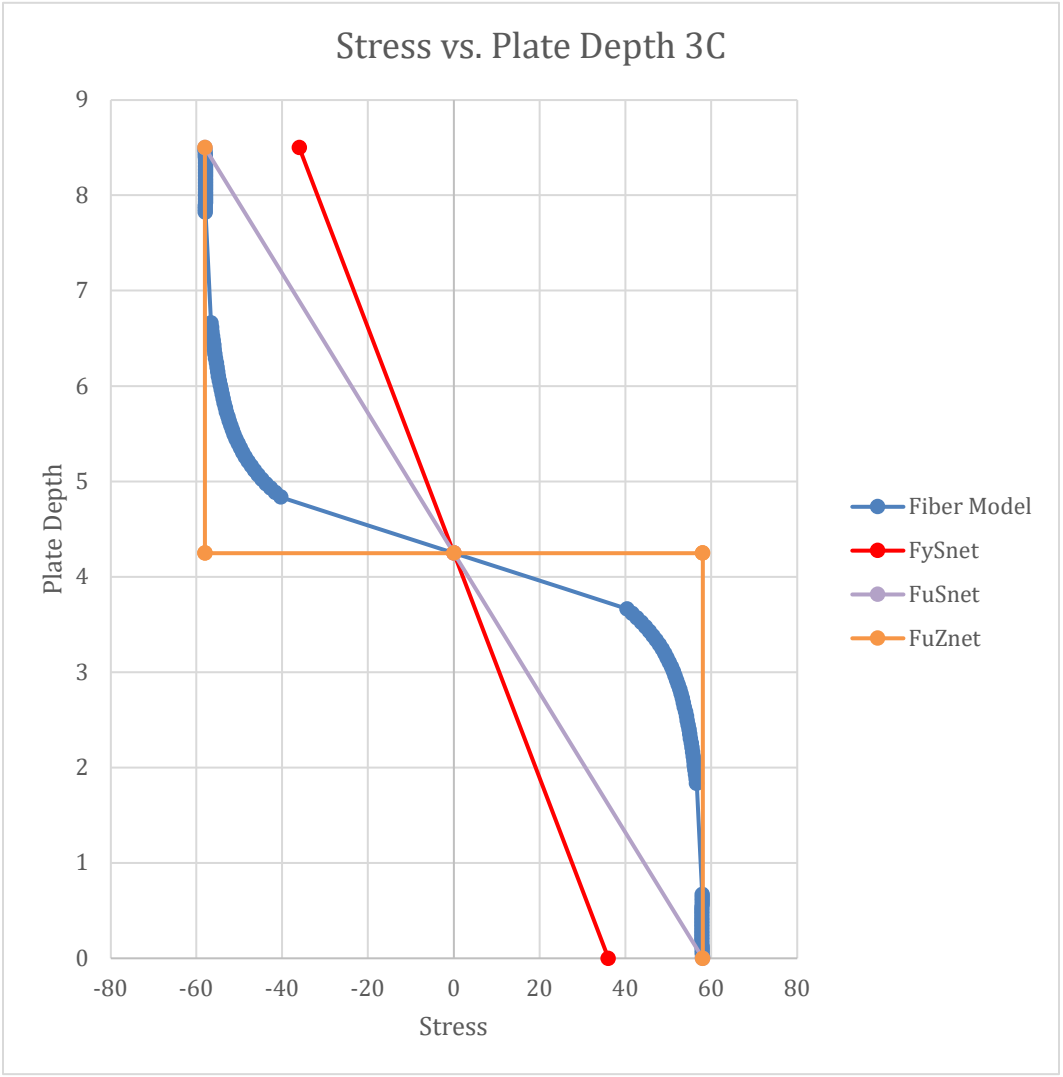
Stress vs. Plate Depth 3C
Plate Depth
9
8
7
6
5
4
3
2
1
0
-80
-60
-40
-20
0
20
40
60
80
Stress
Fiber Model
FySnet
FuSnet
FuZnet

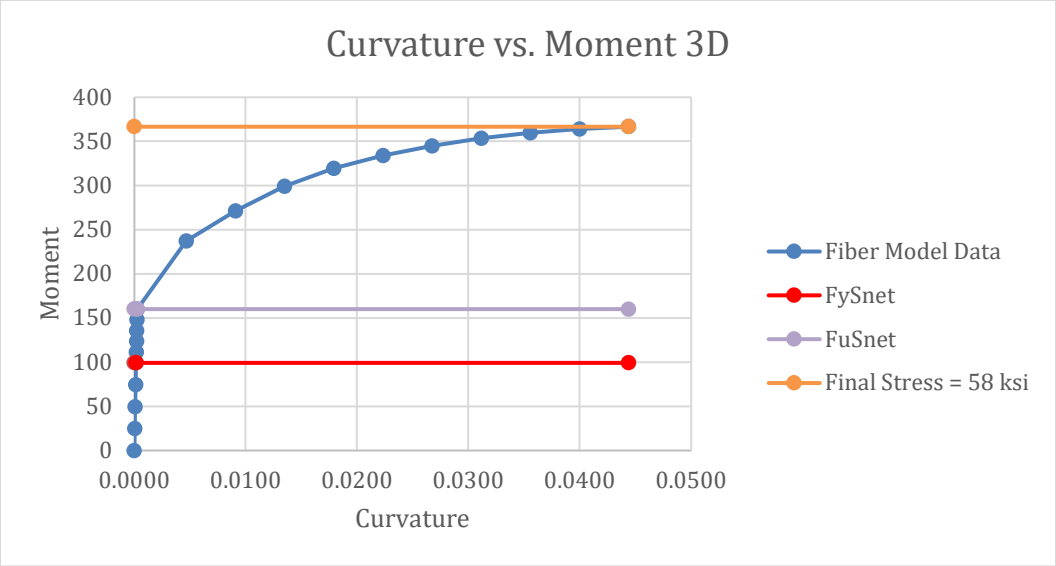
Curvature vs. Moment 3D
Moment
400
350
300
250
200
150
100
50
0
0.0000
0.0100
0.0200
0.0300
0.0400
0.0500
Curvature
Fiber Model Data
FySnet
FuSnet
Final Stress = 58 ksi

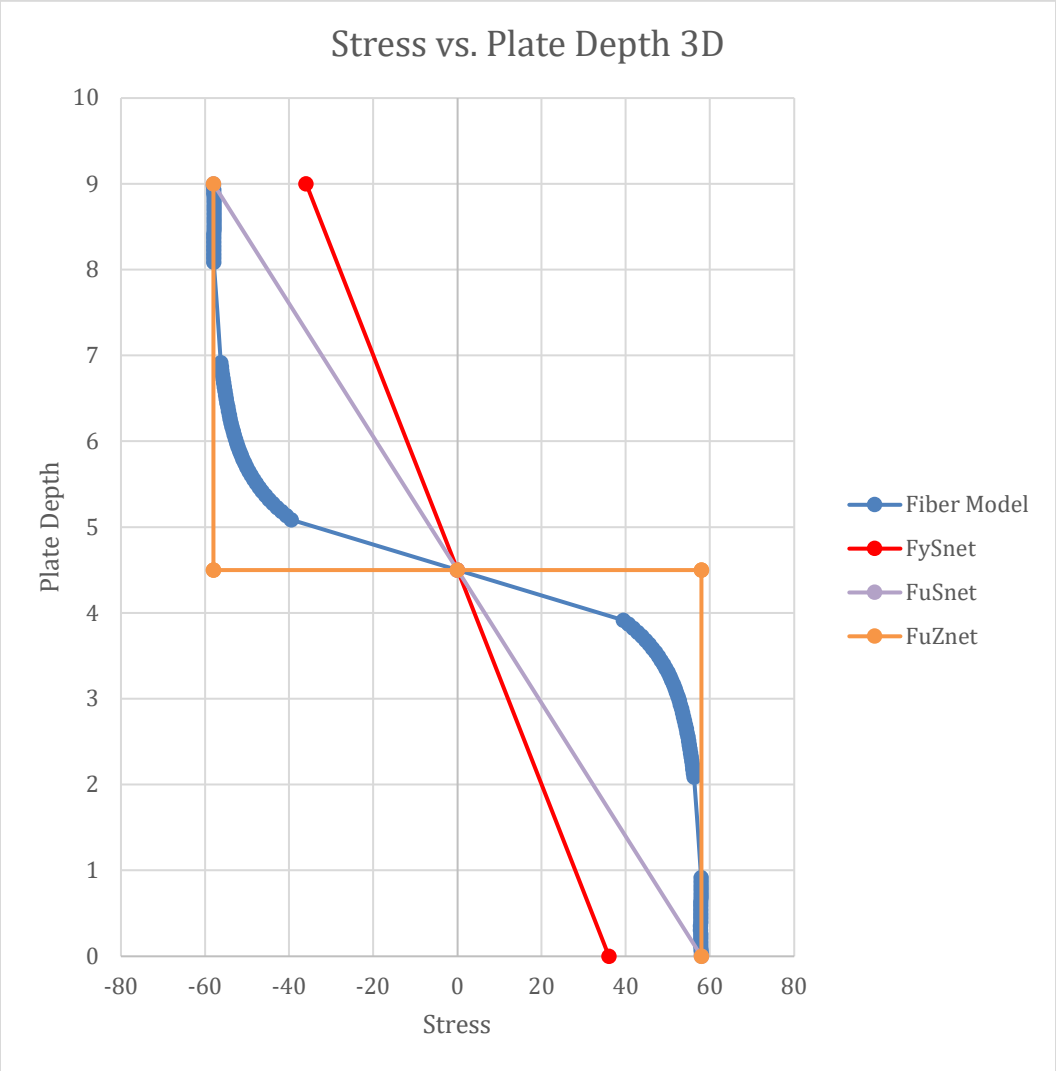
Stress vs. Plate Depth 3D
Plate Depth
10
9
8
7
6
5
4
3
2
1
0
-80
-60
-40
-20
0
20
40
60
80
Stress
Fiber Model
FySnet
FuSnet
FuZnet

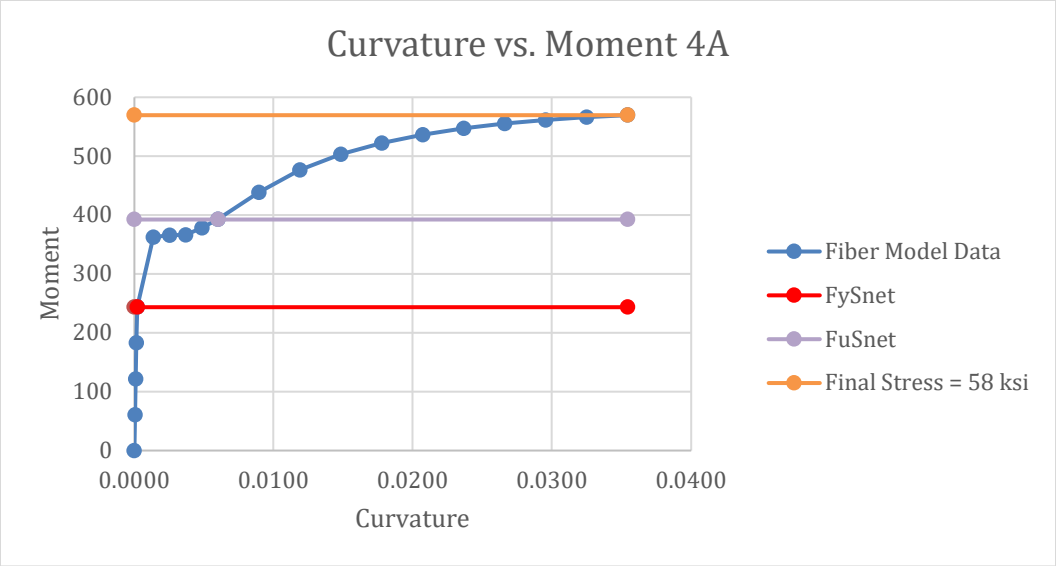
Curvature vs. Moment 4A
Moment
600
500
400
300
200
100
0
0.0000
0.0100
0.0200
0.0300
0.0400
Curvature
Fiber Model Data
FySnet
FuSnet
Final Stress = 58 ksi

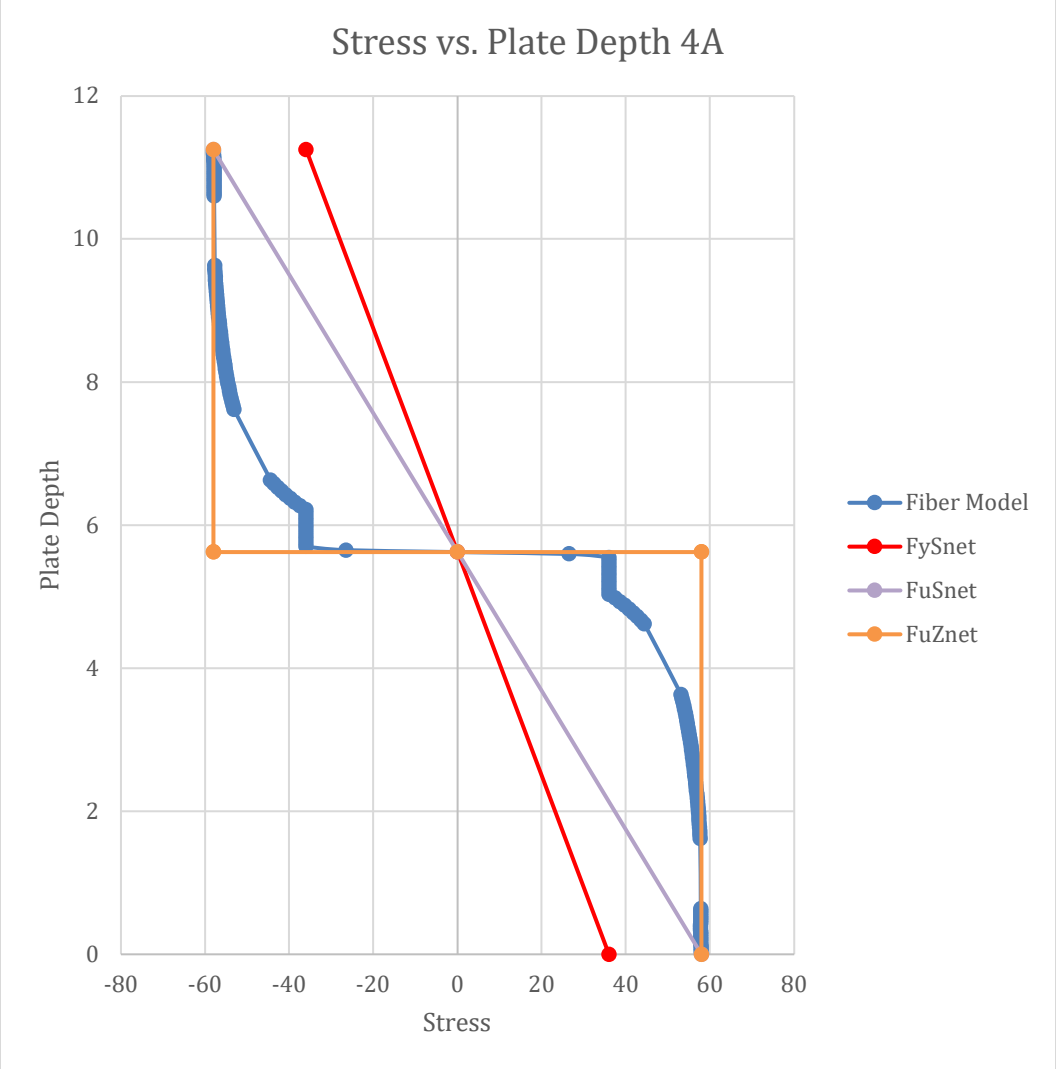
Stress vs. Plate Depth 4A
Plate Depth
12
10
8
6
4
2
0
-80
-60
-40
-20
0
20
40
60
80
Stress
Fiber Model
FySnet
FuSnet
FuZnet

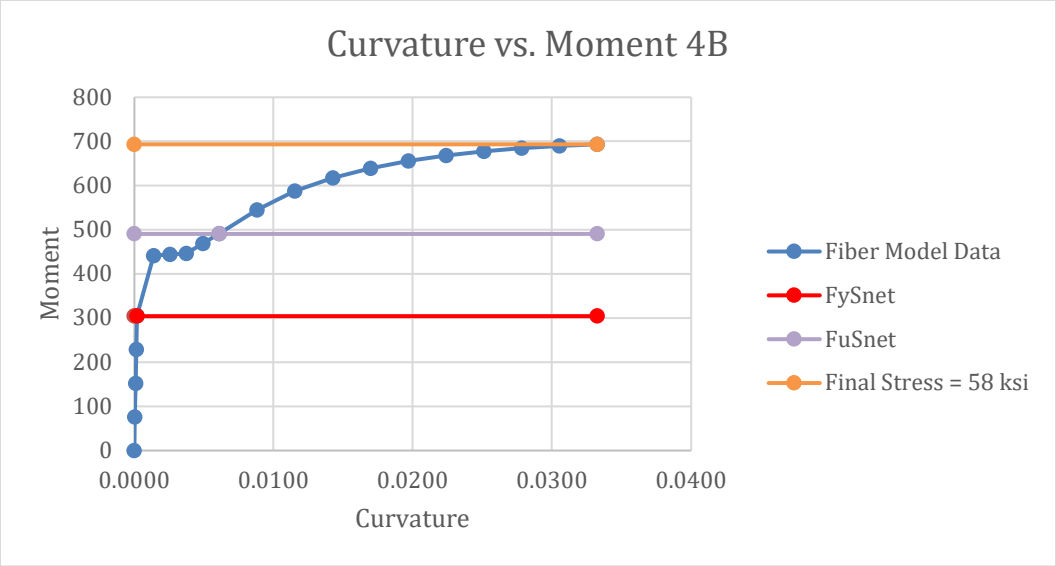
Curvature vs. Moment 4B
Moment
800
700
600
500
400
300
200
100
0
0.0000
0.0100
0.0200
0.0300
0.0400
Curvature
Fiber Model Data
FySnet
FuSnet
Final Stress = 58 ksi

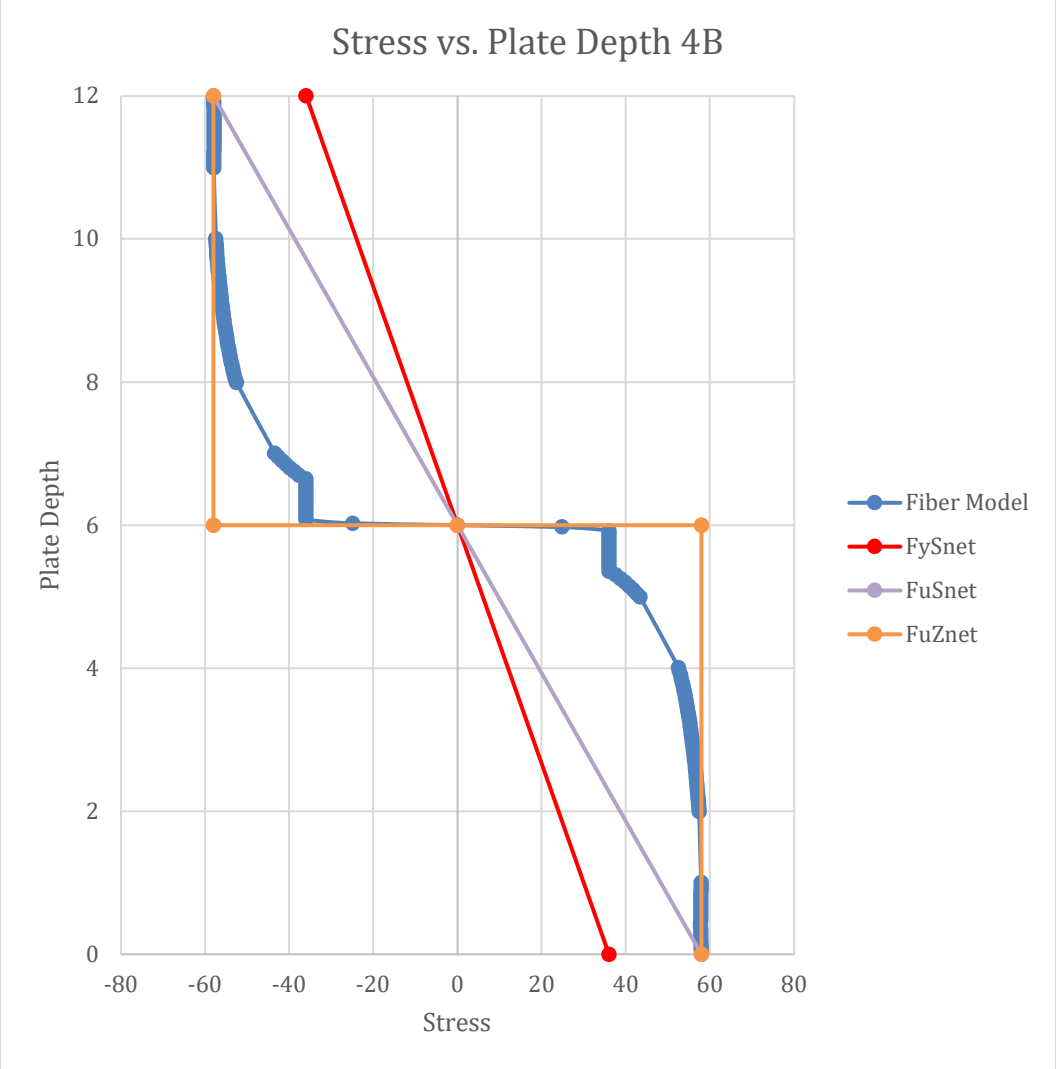
Stress vs. Plate Depth 4B
Plate Depth
12
10
8
6
4
2
0
-80
-60
-40
-20
0
20
40
60
80
Stress
Fiber Model
FySnet
FuSnet
FuZnet

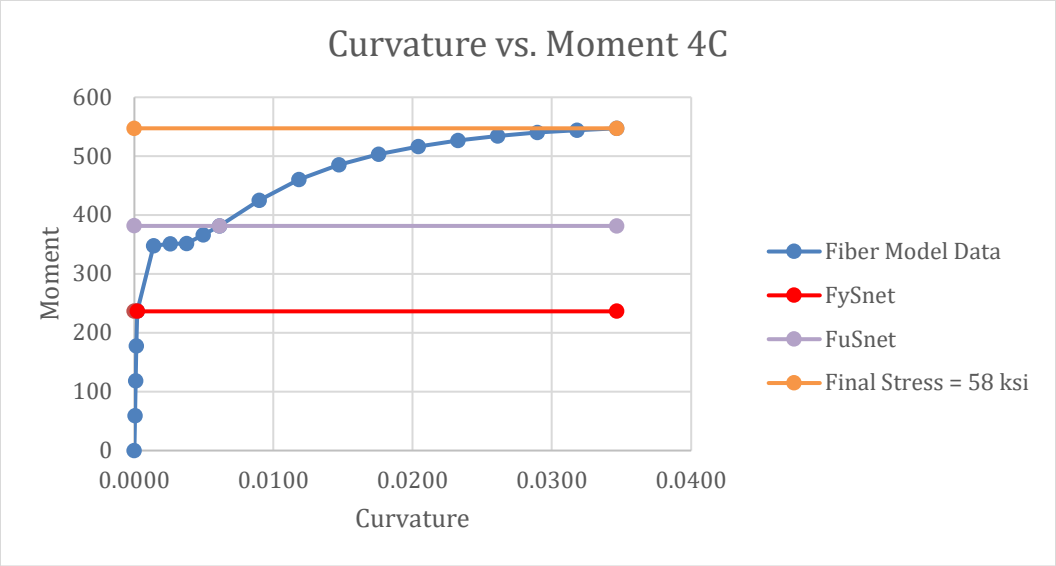
Curvature vs. Moment 4C
600
500
400
300
200
100
0
Moment
0.0000
0.0100
0.0200
0.0300
0.0400
Curvature
Fiber Model Data
FySnet
FuSnet
Final Stress = 58 ksi

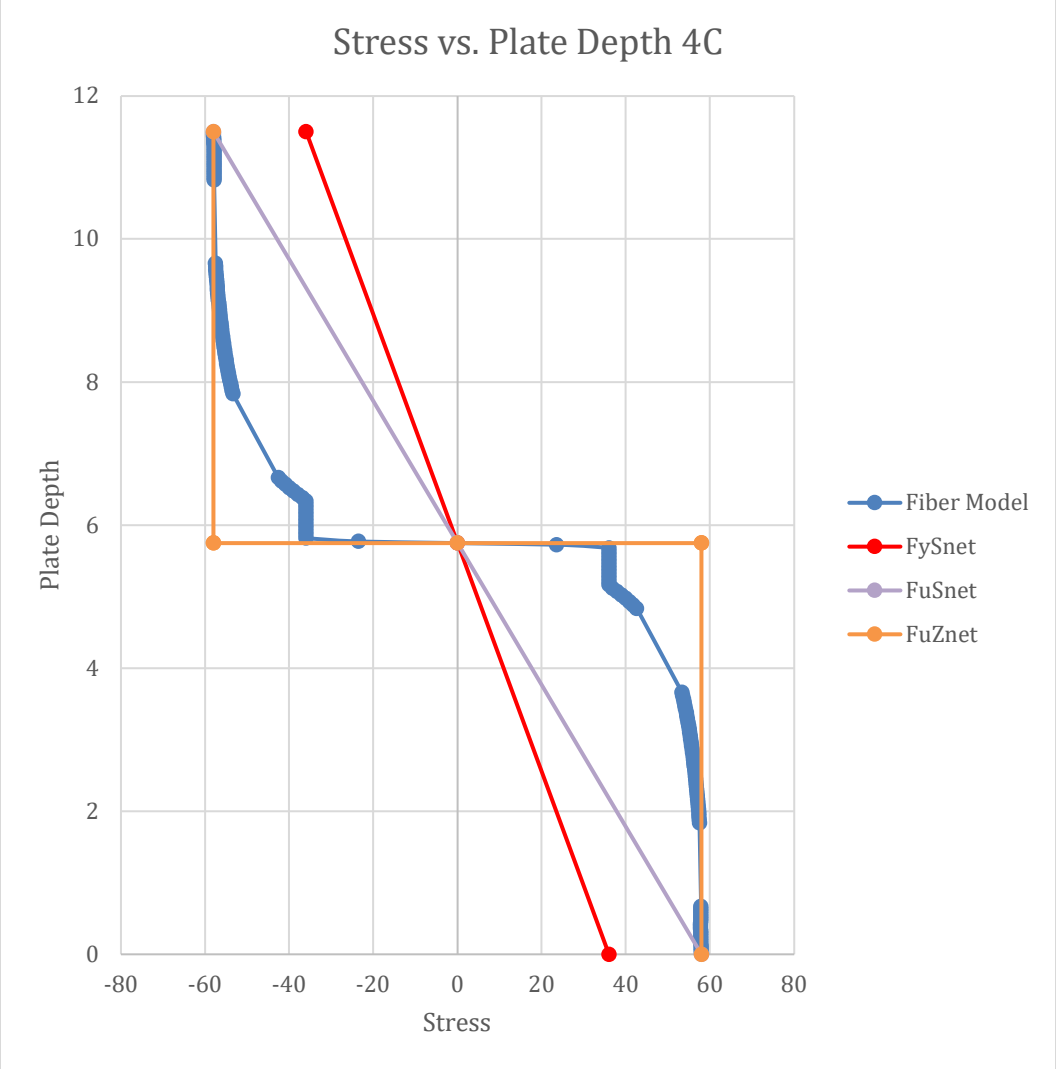
Stress vs. Plate Depth 4C
12
10
8
6
4
2
0
Plate Depth
-80
-60
-40
-20
0
20
40
60
80
Stress
Fiber Model
FySnet
FuSnet
FuZnet

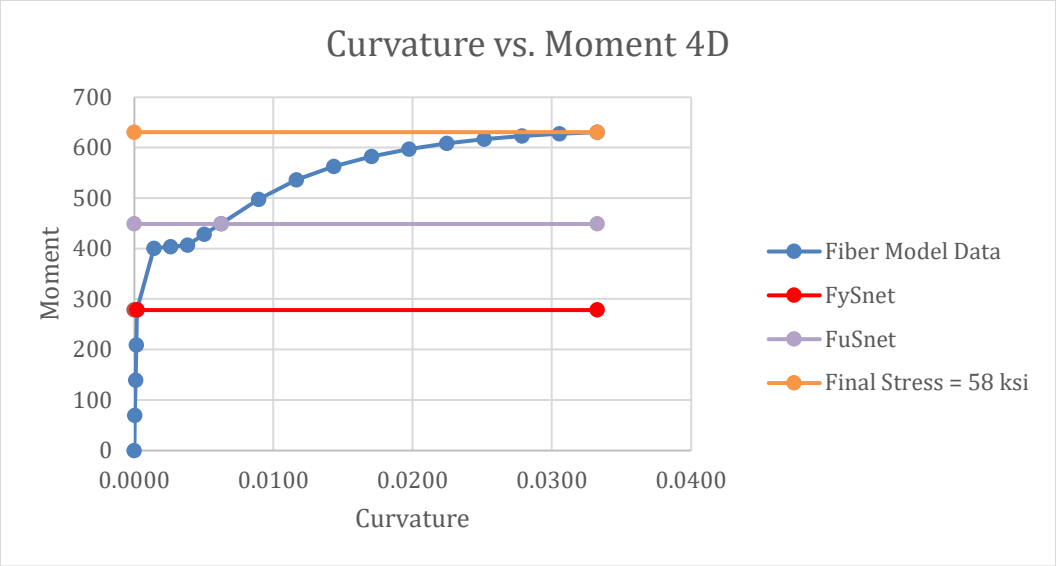
Curvature vs. Moment 4D
Moment
700
600
500
400
300
200
100
0
0.0000
0.0100
0.0200
0.0300
0.0400
Curvature
Fiber Model Data
FySnet
FuSnet
Final Stress = 58 ksi

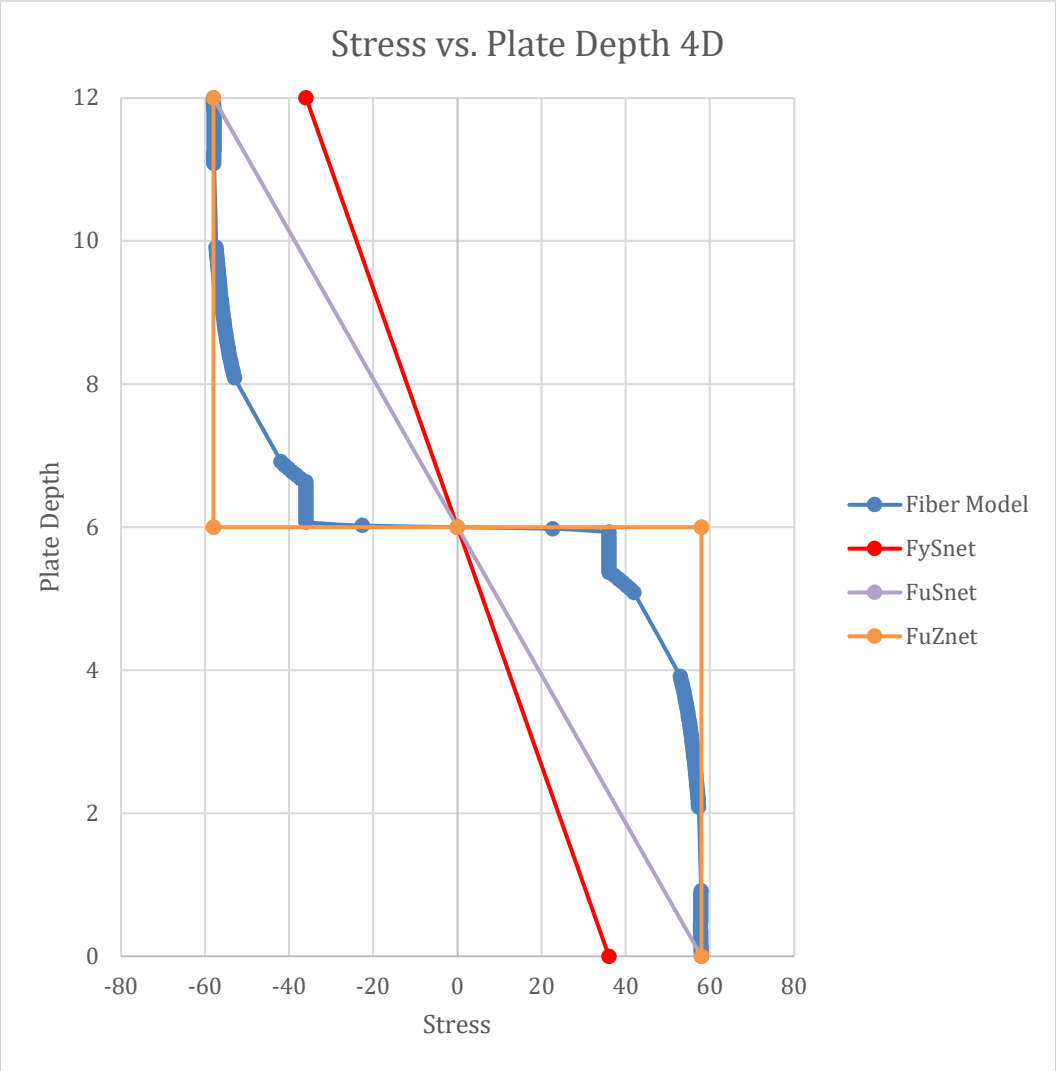
Stress vs. Plate Depth 4D
Plate Depth
12
10
8
6
4
2
0
-80
-60
-40
-20
0
20
40
60
80
Stress
Fiber Model
FySnet
FuSnet
FuZnet

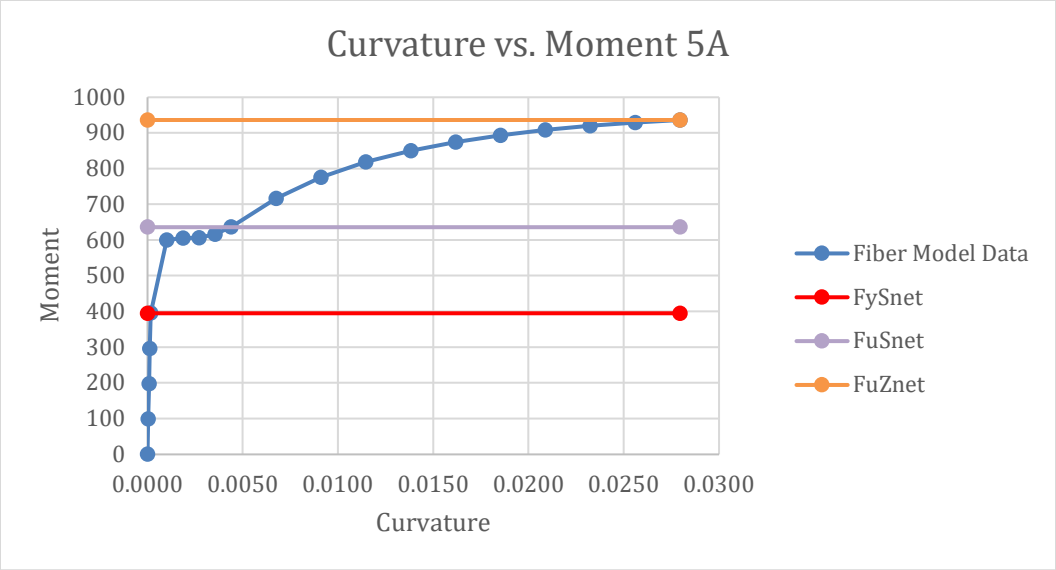
Curvature vs. Moment 5A
Moment
1000
900
800
700
600
500
400
300
200
100
0
0.0000
0.0050
0.0100
0.0150
0.0200
0.0250
0.0300
Curvature
Fiber Model Data
FySnet
FuSnet
FuZnet

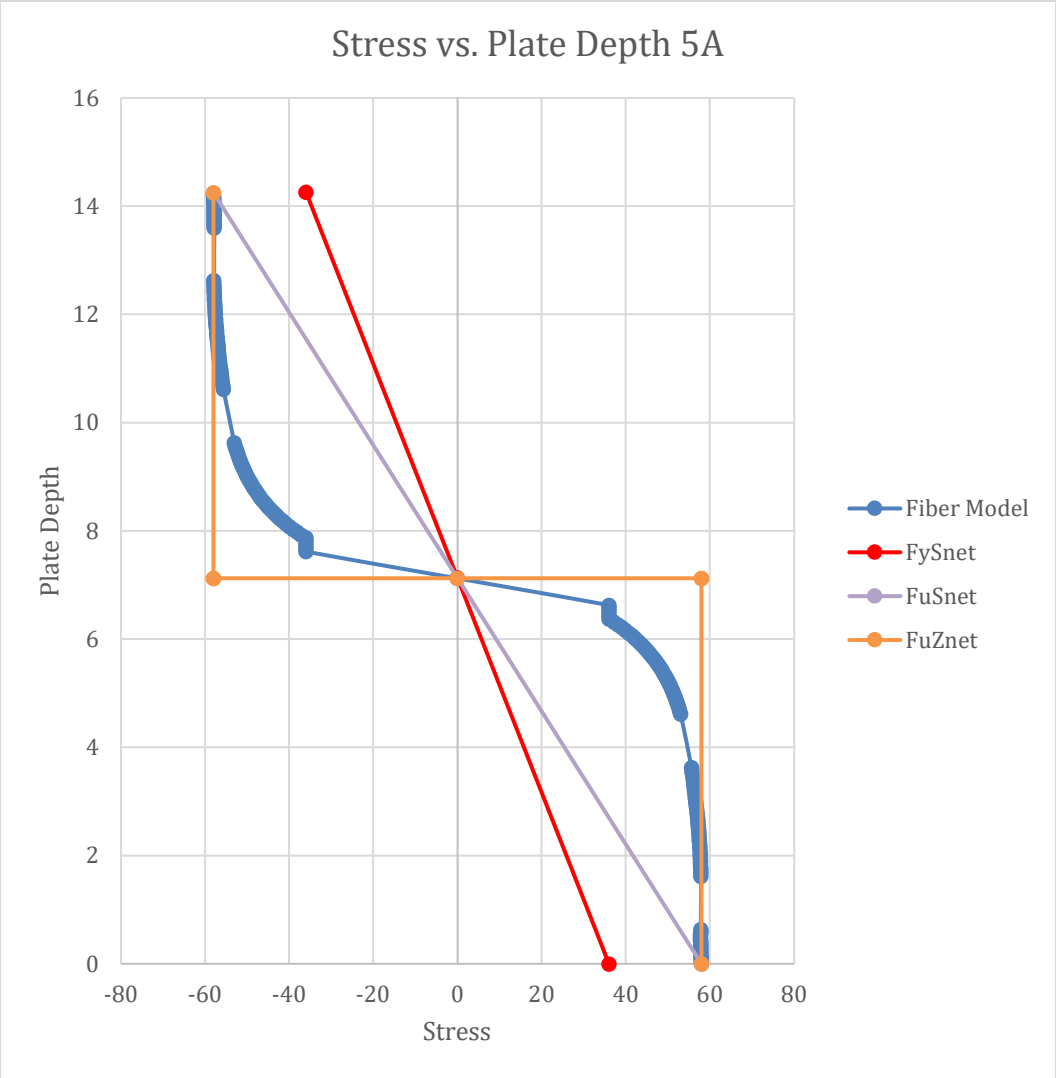
Stress vs. Plate Depth 5A
Plate Depth
16
14
12
10
8
6
4
2
0
-80
-60
-40
-20
0
20
40
60
80
Stress
Fiber Model
FySnet
FuSnet
FuZnet

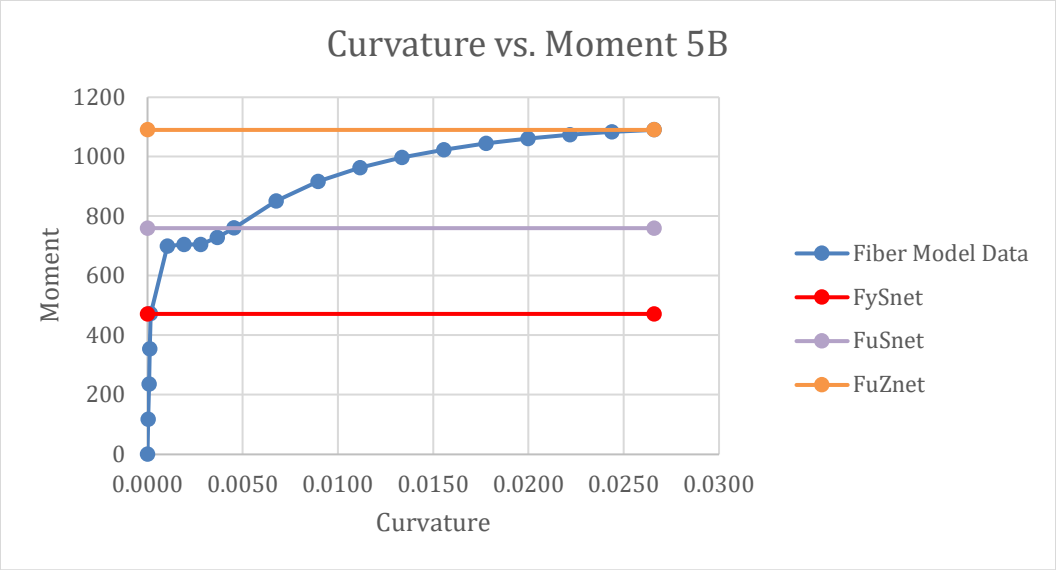
Curvature vs. Moment 5B
Moment
1200
1000
800
600
400
200
0
0.0000
0.0050
0.0100
0.0150
0.0200
0.0250
0.0300
Curvature
Fiber Model Data
FySnet
FuSnet
FuZnet

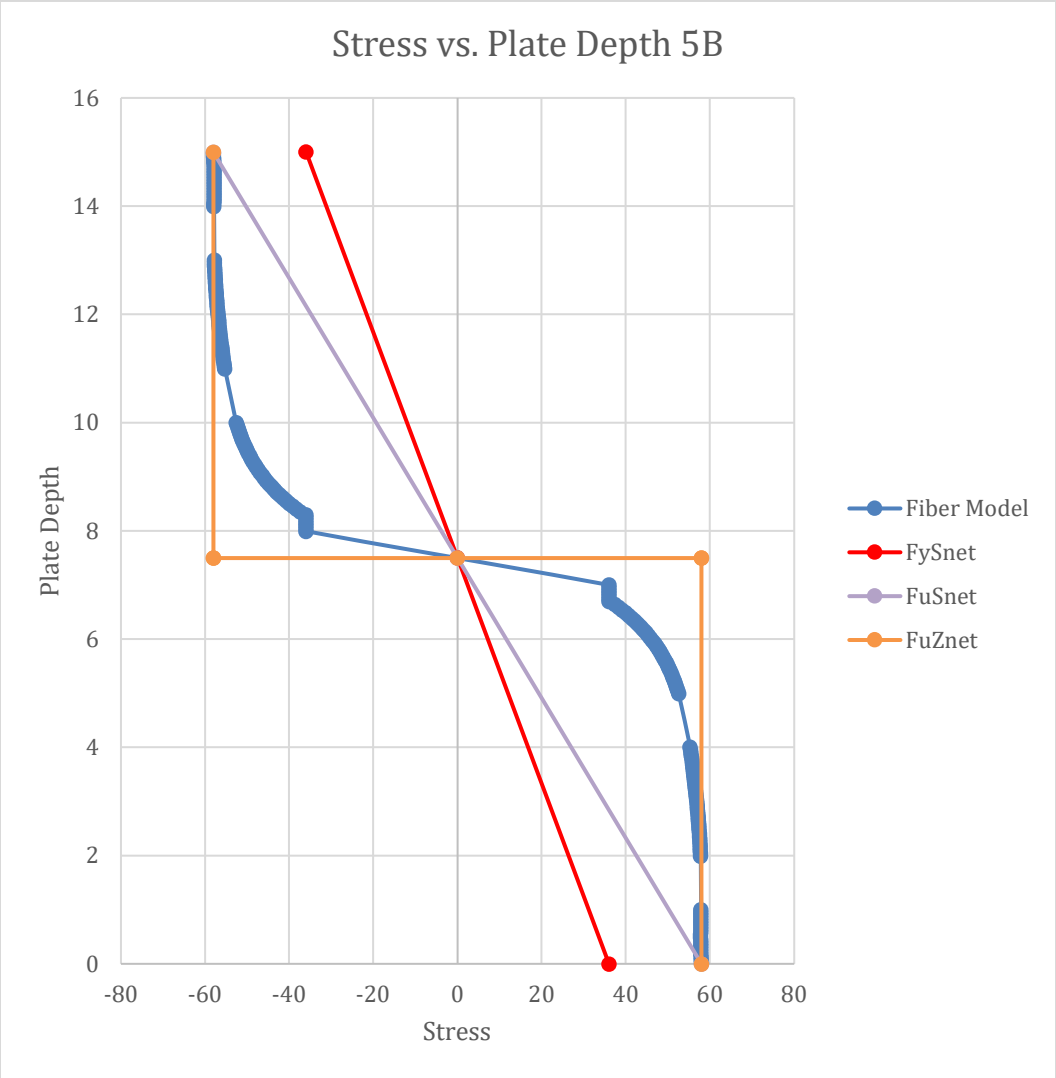
Stress vs. Plate Depth 5B
Plate Depth
16
14
12
10
8
6
4
2
0
-80
-60
-40
-20
0
20
40
60
80
Stress
Fiber Model
FySnet
FuSnet
FuZnet

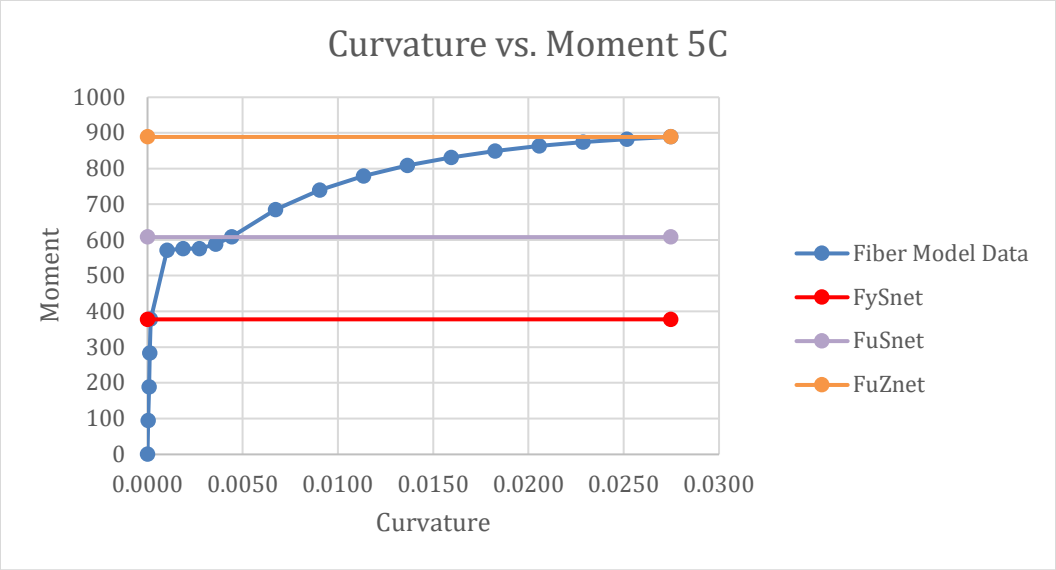
Curvature vs. Moment 5C
Moment
1000
900
800
700
600
500
400
300
200
100
0
0.0000
0.0050
0.0100
0.0150
0.0200
0.0250
0.0300
Curvature
Fiber Model Data
FySnet
FuSnet
FuZnet

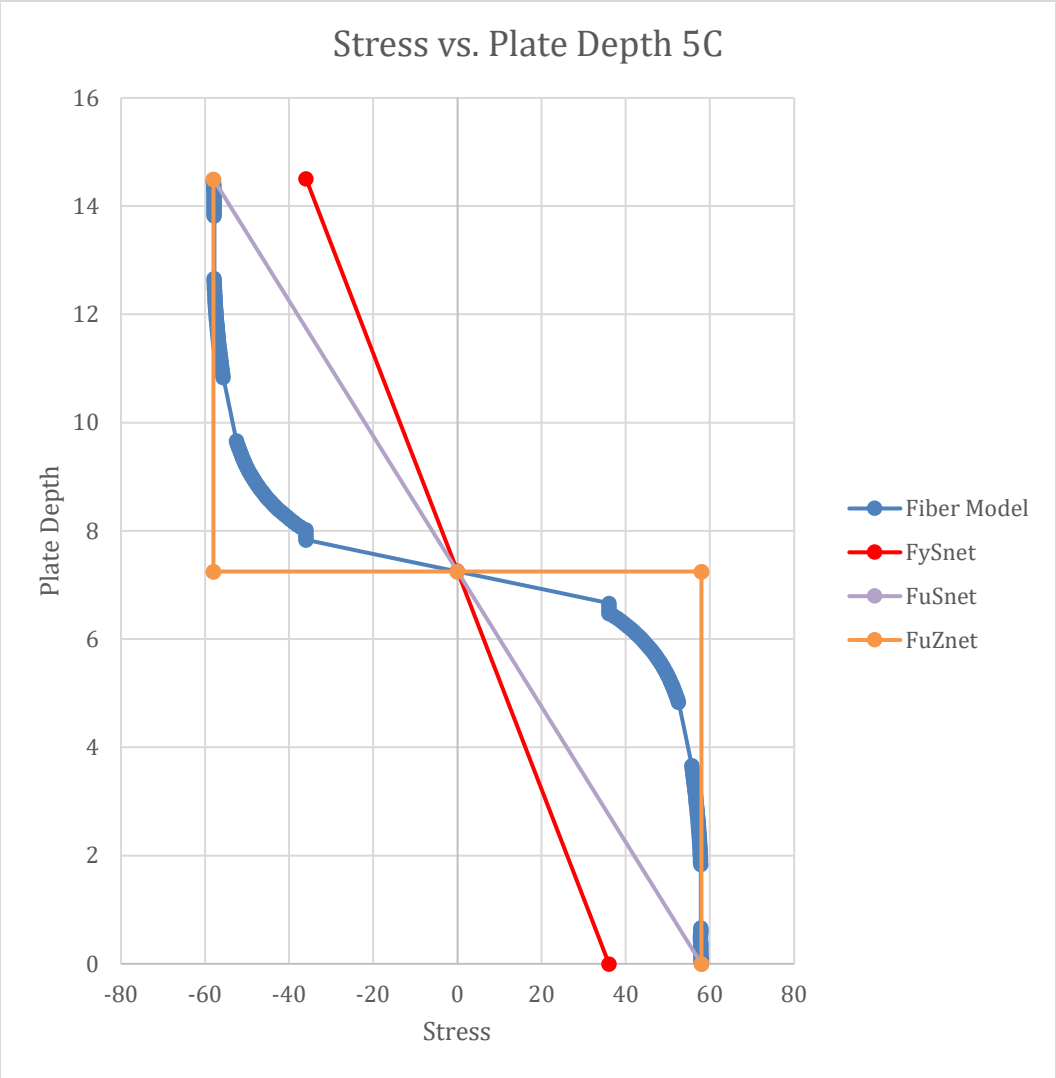
Stress vs. Plate Depth 5C
Plate Depth
16
14
12
10
8
6
4
2
0
-80
-60
-40
-20
0
20
40
60
80
Stress
Fiber Model
FySnet
FuSnet
FuZnet

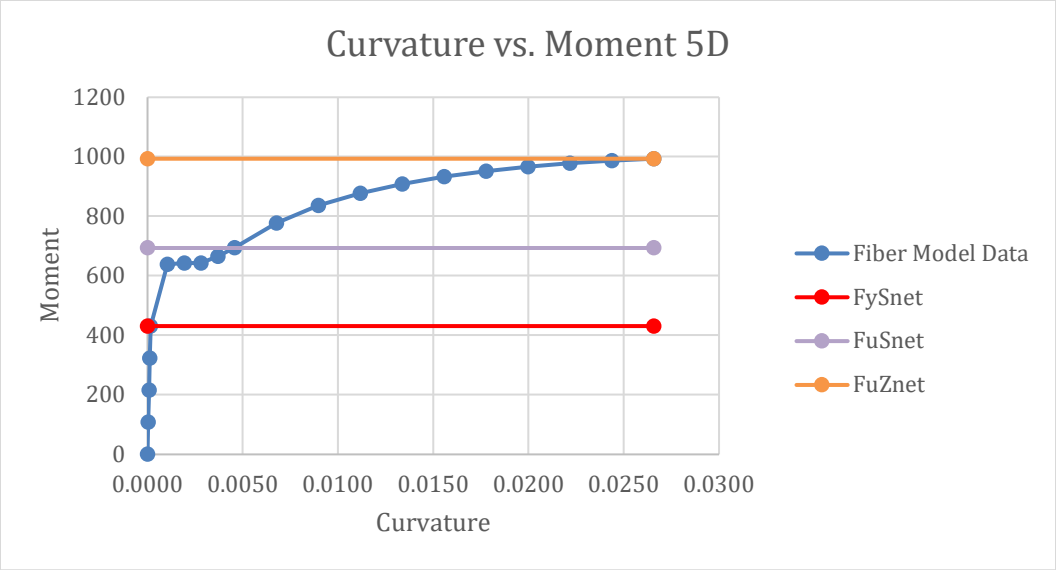
Curvature vs. Moment 5D
Moment
Curvature
1200
1000
800
600
400
200
0
0.0000
0.0050
0.0100
0.0150
0.0200
0.0250
0.0300
Fiber Model Data
FySnet
FuSnet
FuZnet

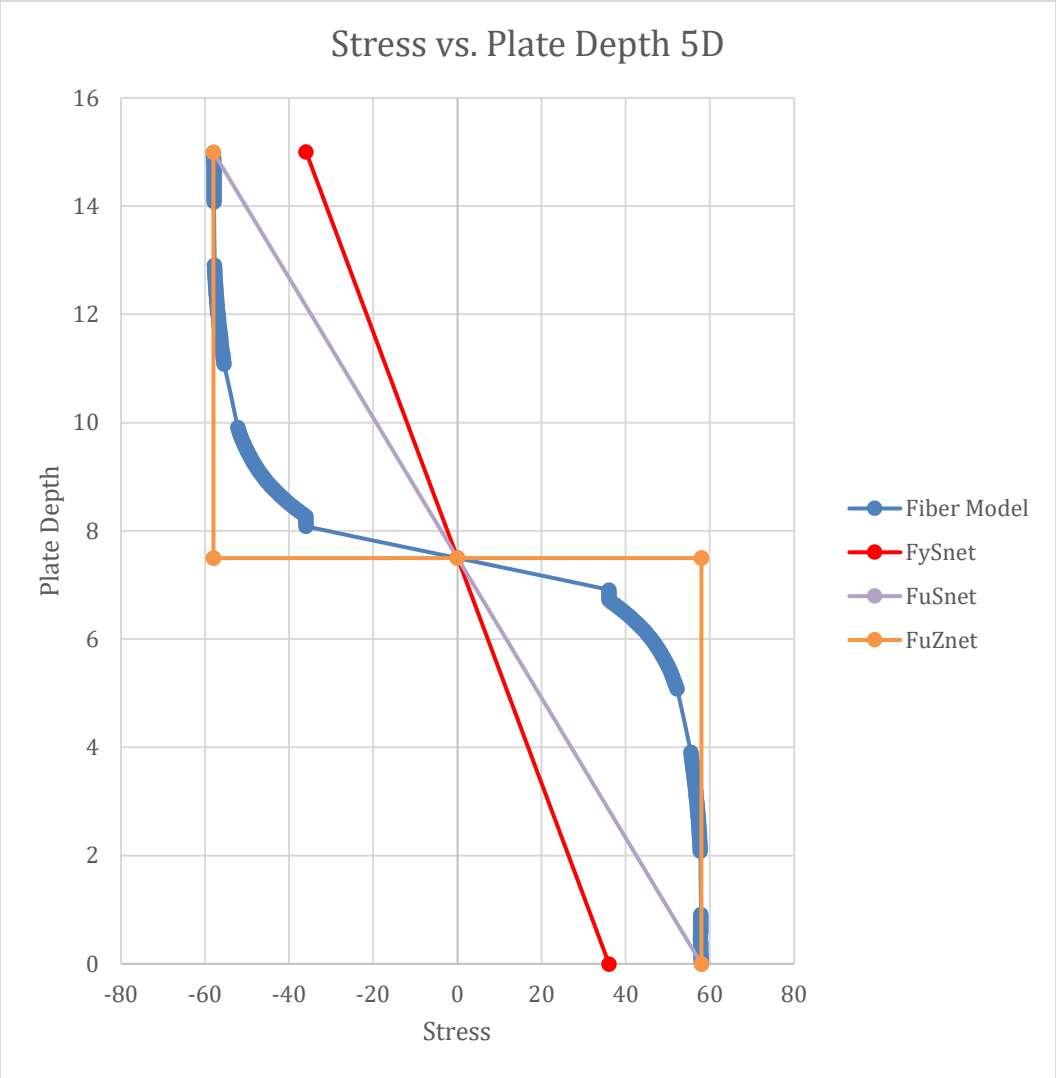
Stress vs. Plate Depth 5D
Plate Depth
Stress
16
14
12
10
8
6
4
2
0
-80
-60
-40
-20
0
20
40
60
80
Fiber Model
FySnet
FuSnet
FuZnet

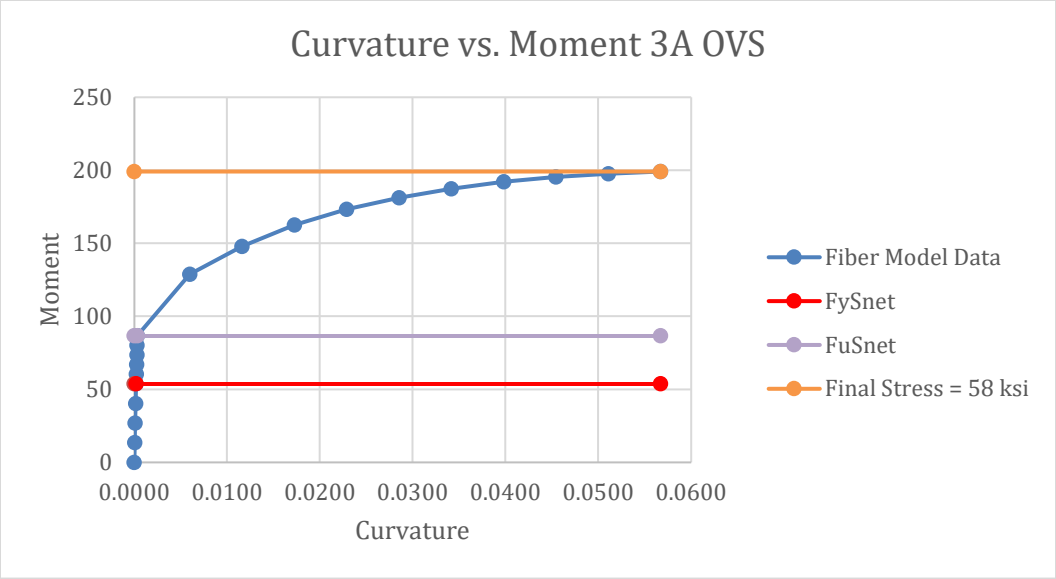
Curvature vs. Moment 3A OVS
Moment
250
200
150
100
50
0
0.0000
0.0100
0.0200
0.0300
0.0400
0.0500
0.0600
Curvature
Fiber Model Data
FySnet
FuSnet
Final Stress = 58 ksi

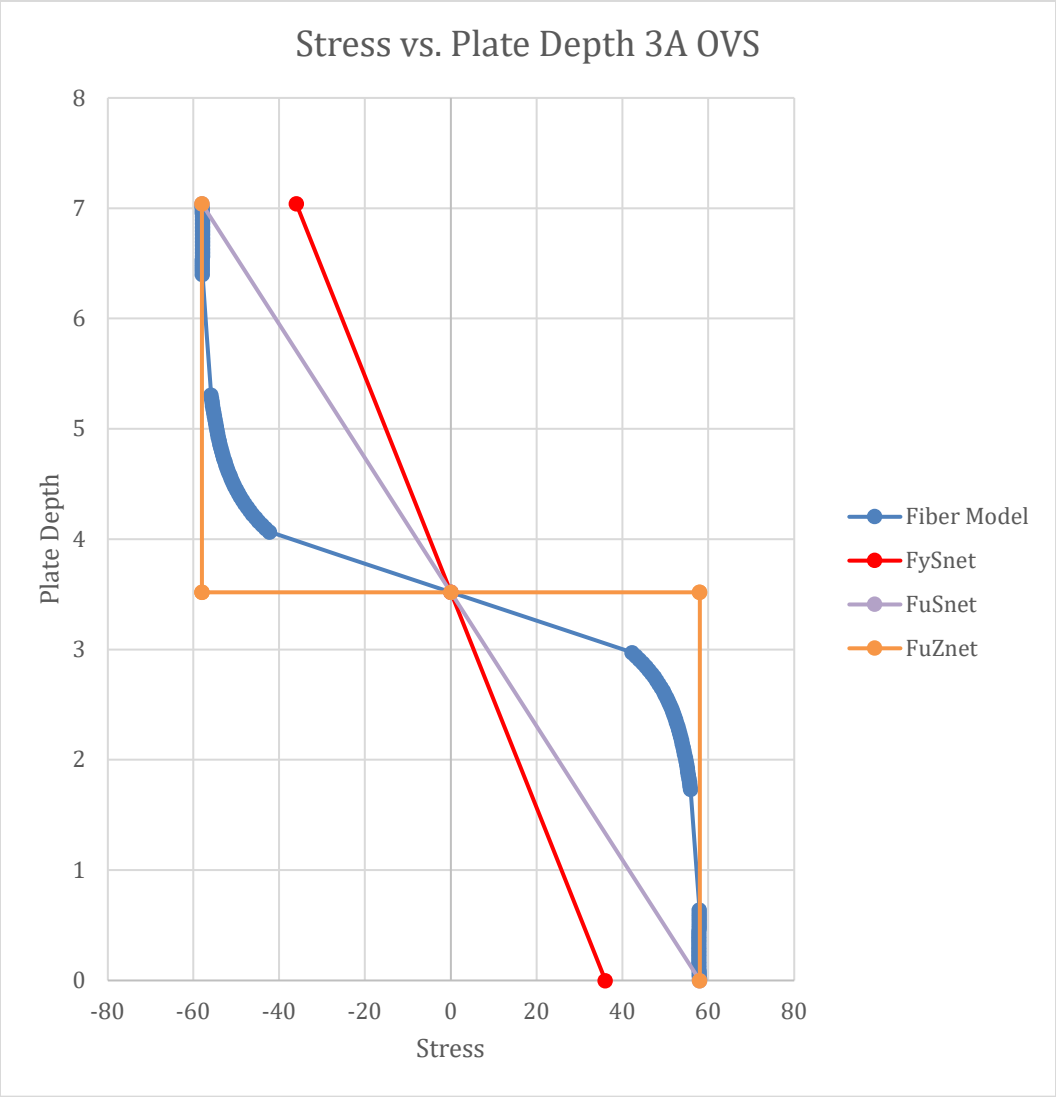
Stress vs. Plate Depth 3A OVS
Plate Depth
8
7
6
5
4
3
2
1
0
-80
-60
-40
-20
0
20
40
60
80
Stress
Fiber Model
FySnet
FuSnet
FuZnet

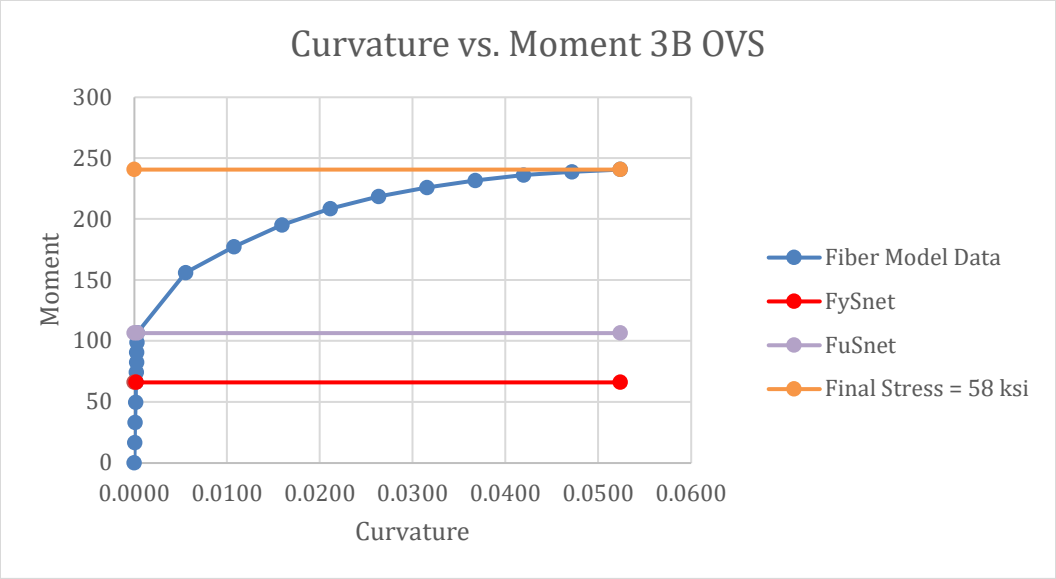
Curvature vs. Moment 3B OVS
Moment
300
250
200
150
100
50
0
0.0000
0.0100
0.0200
0.0300
0.0400
0.0500
0.0600
Curvature
Fiber Model Data
FySnet
FuSnet
Final Stress = 58 ksi


Stress vs. Plate Depth 3B OVS
Plate Depth
9
8
7
6
5
4
3
2
1
0
-80
-60
-40
-20
0
20
40
60
80
Stress
Fiber Model
FySnet
FuSnet
FuZnet

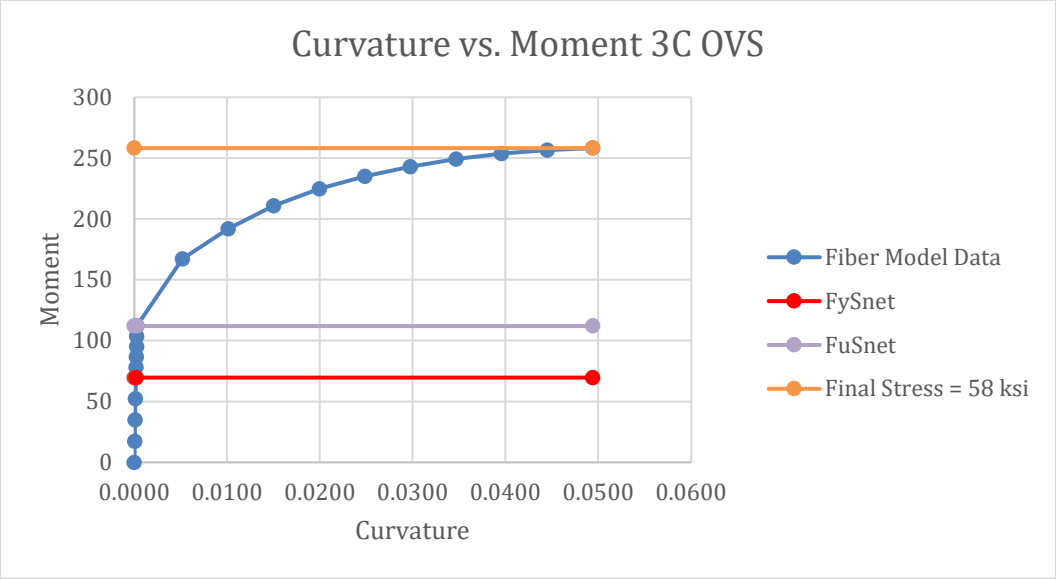
Curvature vs. Moment 3C OVS
Moment
300
250
200
150
100
50
0
0.0000
0.0100
0.0200
0.0300
0.0400
0.0500
0.0600
Curvature
Fiber Model Data
FySnet
FuSnet
Final Stress = 58 ksi

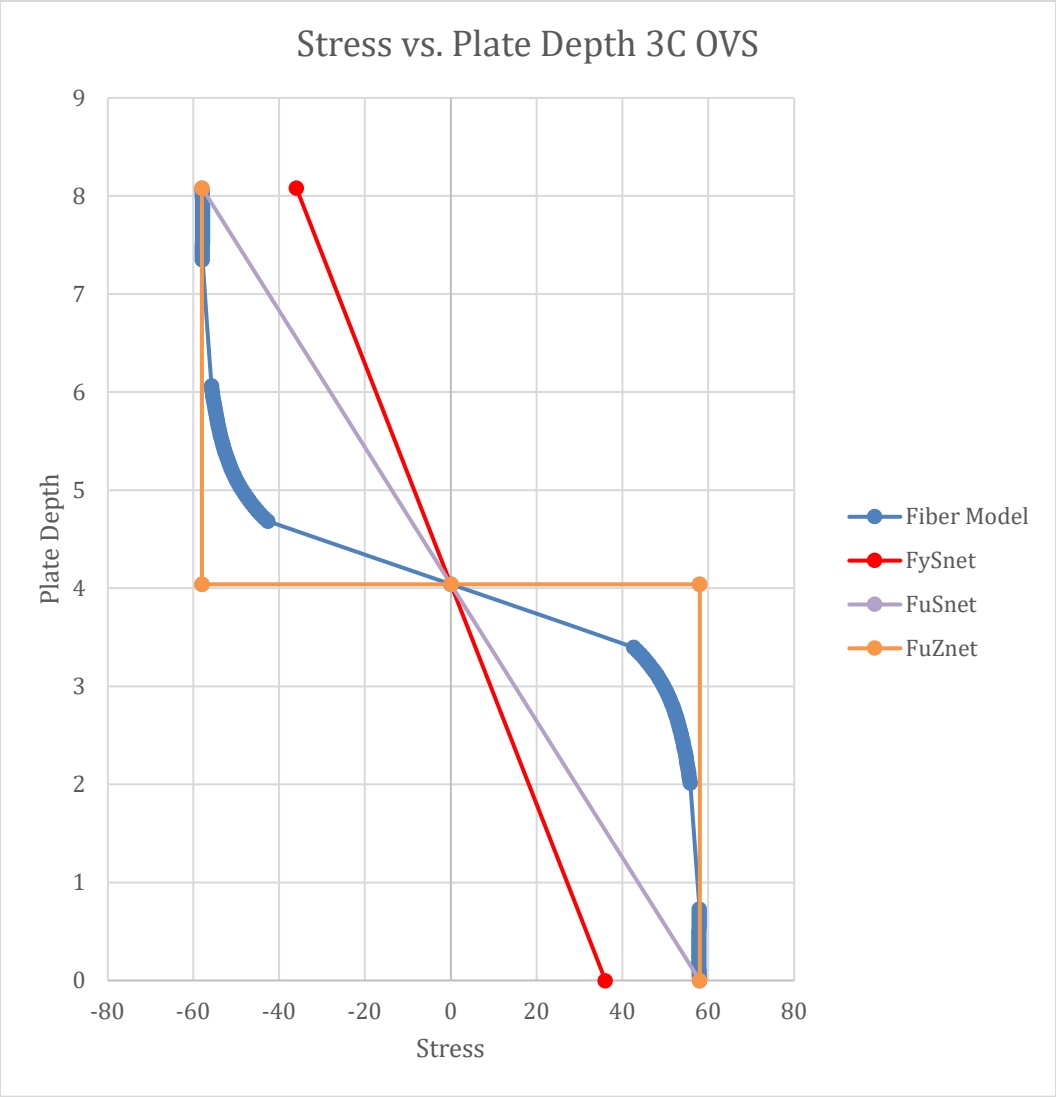
Stress vs. Plate Depth 3C OVS
Plate Depth
9
8
7
6
5
4
3
2
1
0
-80
-60
-40
-20
0
20
40
60
80
Stress
Fiber Model
FySnet
FuSnet
FuZnet

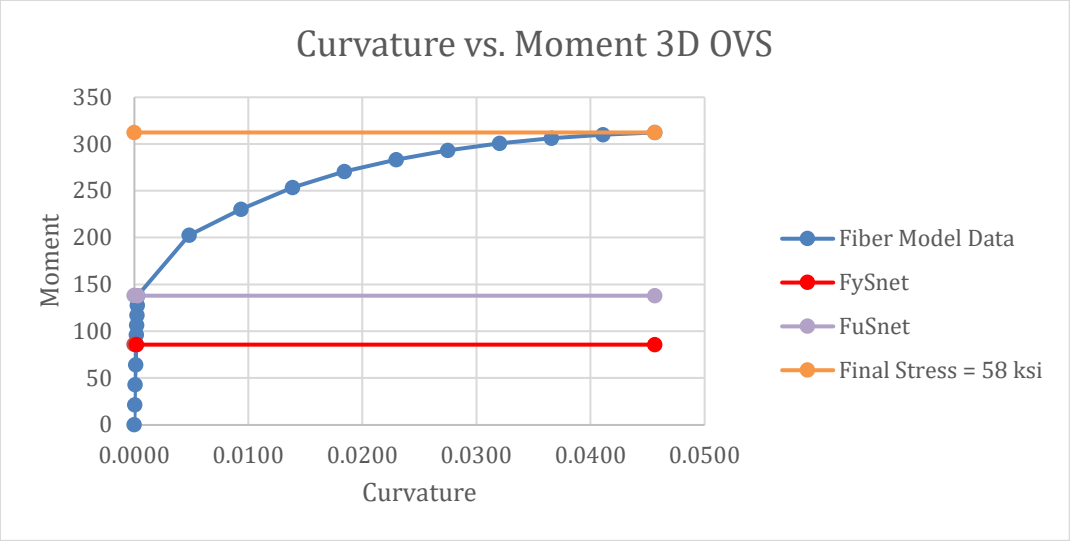
Curvature vs. Moment 3D OVS
Moment
350
300
250
200
150
100
50
0
0.0000
0.0100
0.0200
0.0300
0.0400
0.0500
Curvature
Fiber Model Data
FySnet
FuSnet
Final Stress = 58 ksi

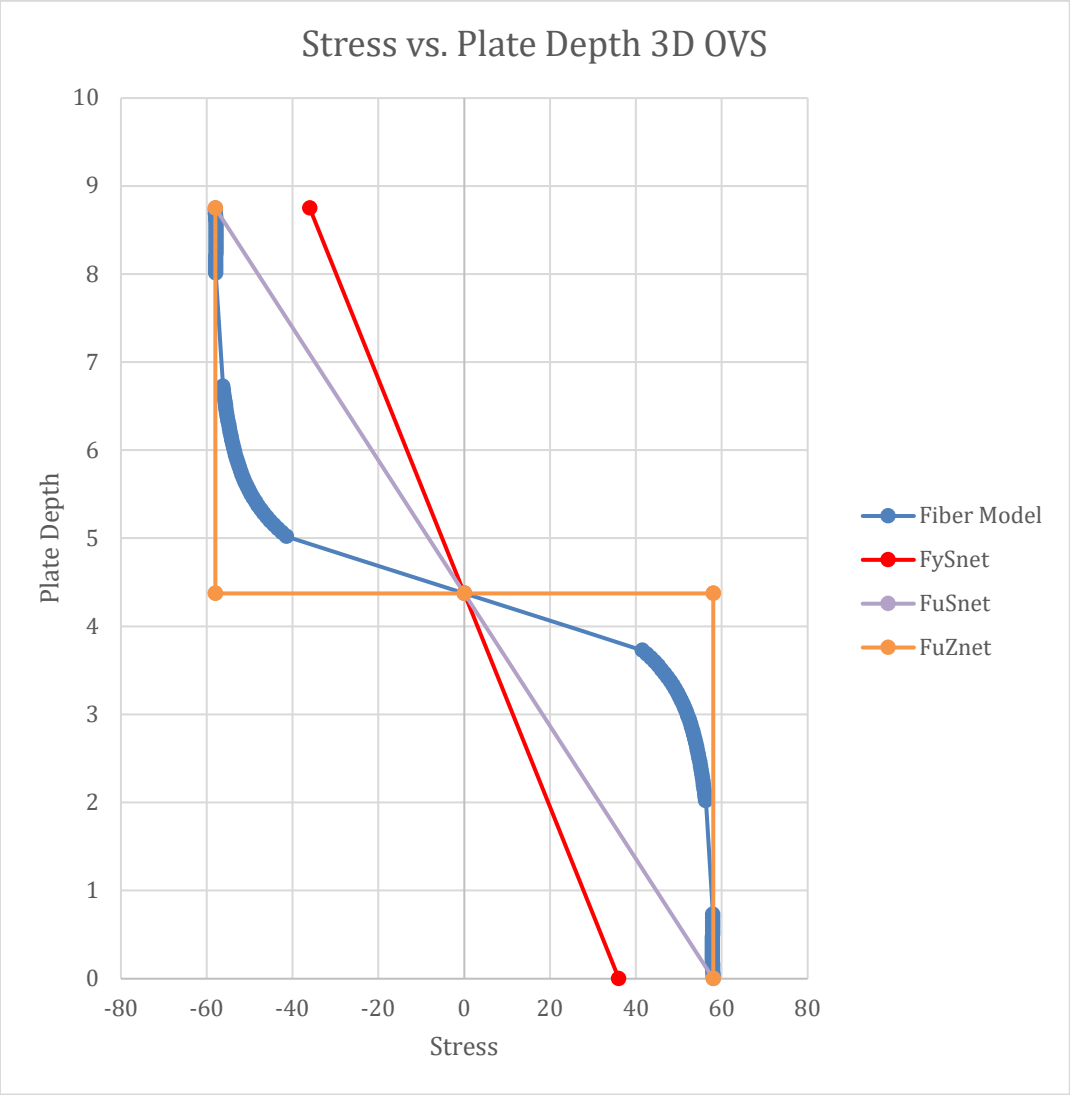
Stress vs. Plate Depth 3D OVS
Plate Depth
10
9
8
7
6
5
4
3
2
1
0
-80
-60
-40
-20
0
20
40
60
80
Stress
Fiber Model
FySnet
FuSnet
FuZnet

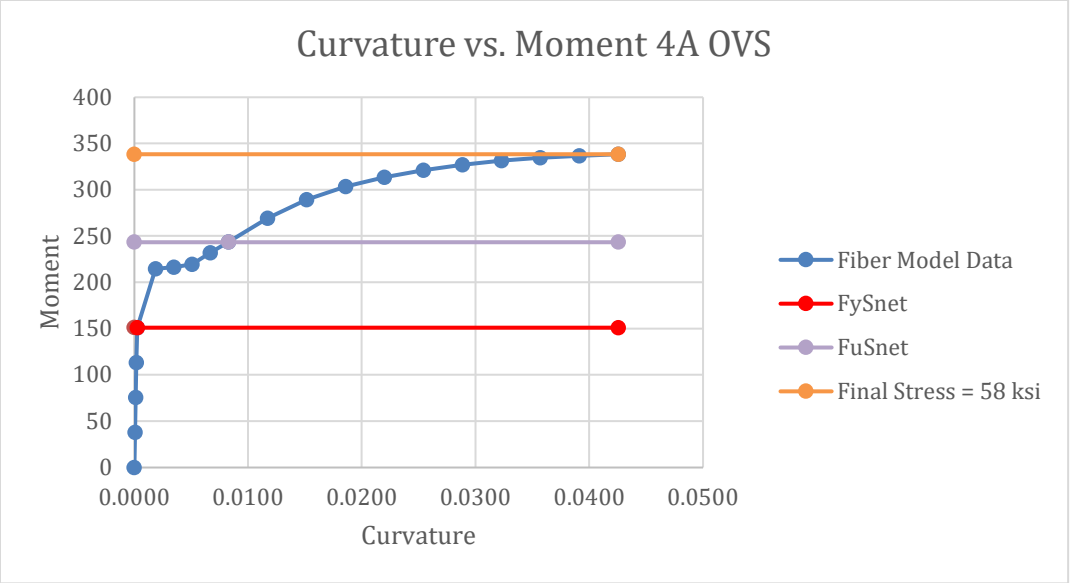
Curvature vs. Moment 4A OVS
Moment
400
350
300
250
200
150
100
50
0
0.0000
0.0100
0.0200
0.0300
0.0400
0.0500
Curvature
Fiber Model Data
FySnet
FuSnet
Final Stress = 58 ksi

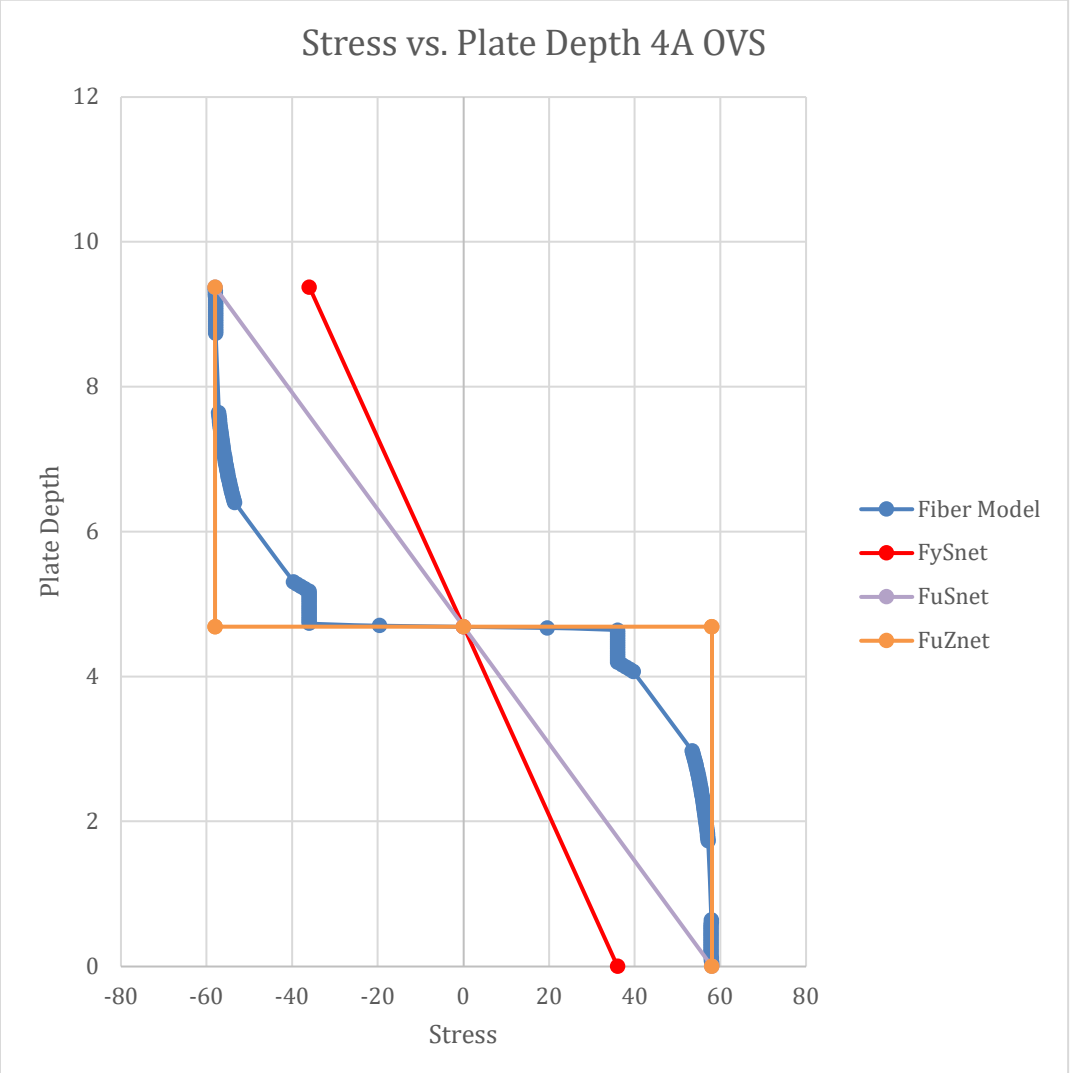
Stress vs. Plate Depth 4A OVS
Plate Depth
12
10
8
6
4
2
0
-80
-60
-40
-20
0
20
40
60
80
Stress
Fiber Model
FySnet
FuSnet
FuZnet

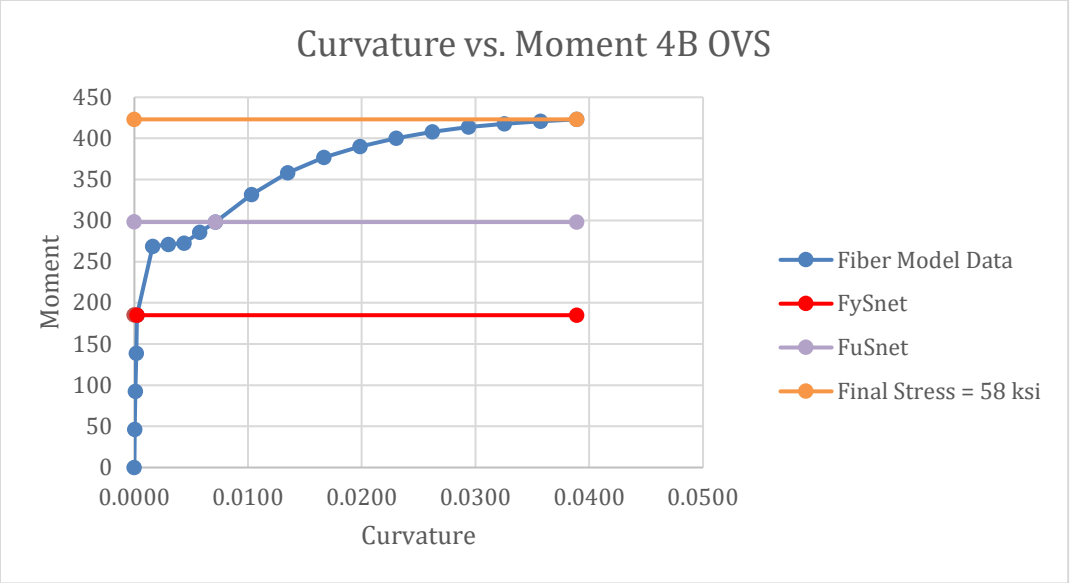
Curvature vs. Moment 4B OVS
Moment
Curvature
0
50
100
150
200
250
300
350
400
450
0.0000
0.0100
0.0200
0.0300
0.0400
0.0500
Fiber Model Data
FySnet
FuSnet
Final Stress = 58 ksi

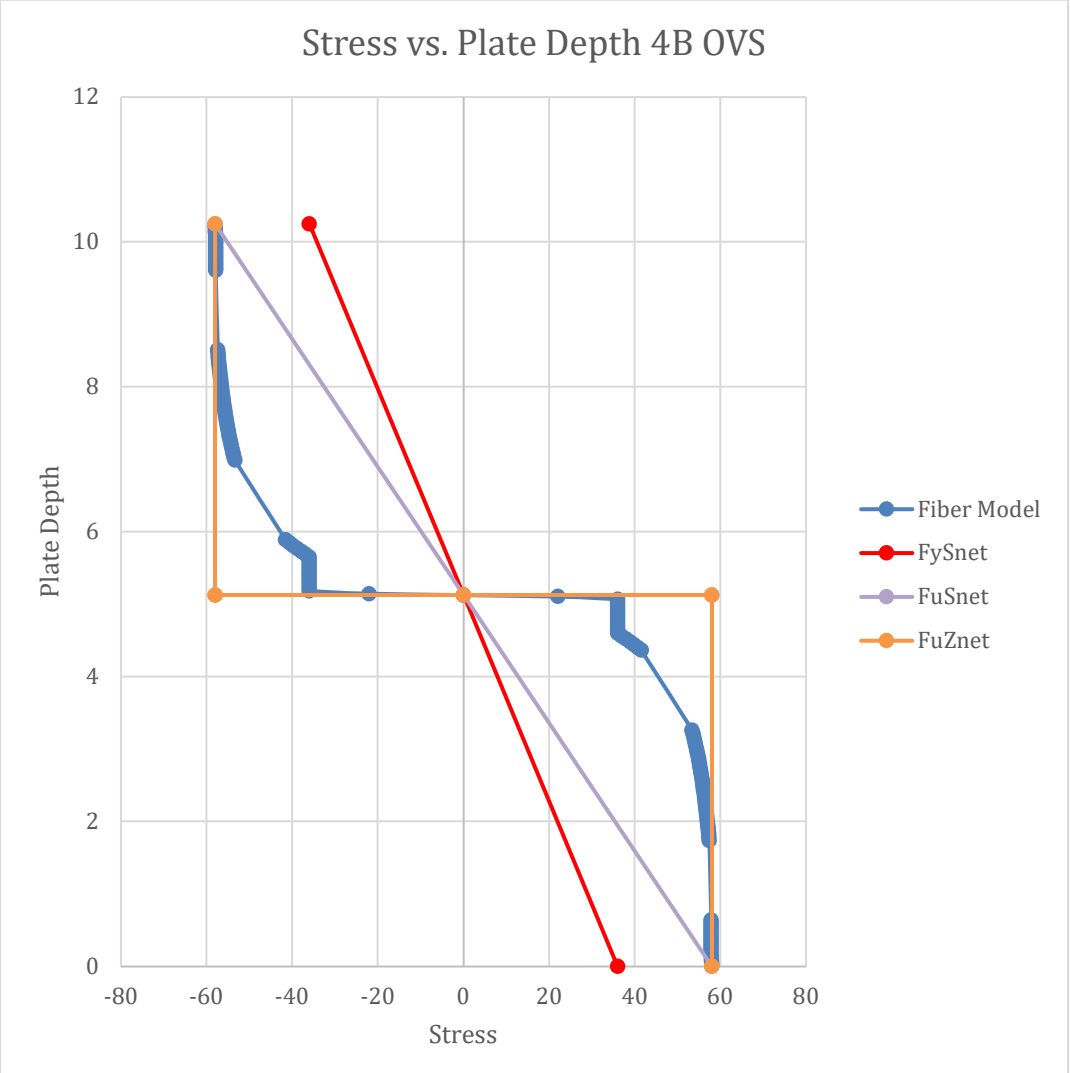
Stress vs. Plate Depth 4B OVS
Plate Depth
Stress
0
2
4
6
8
10
12
-80
-60
-40
-20
0
20
40
60
80
Fiber Model
FySnet
FuSnet
FuZnet

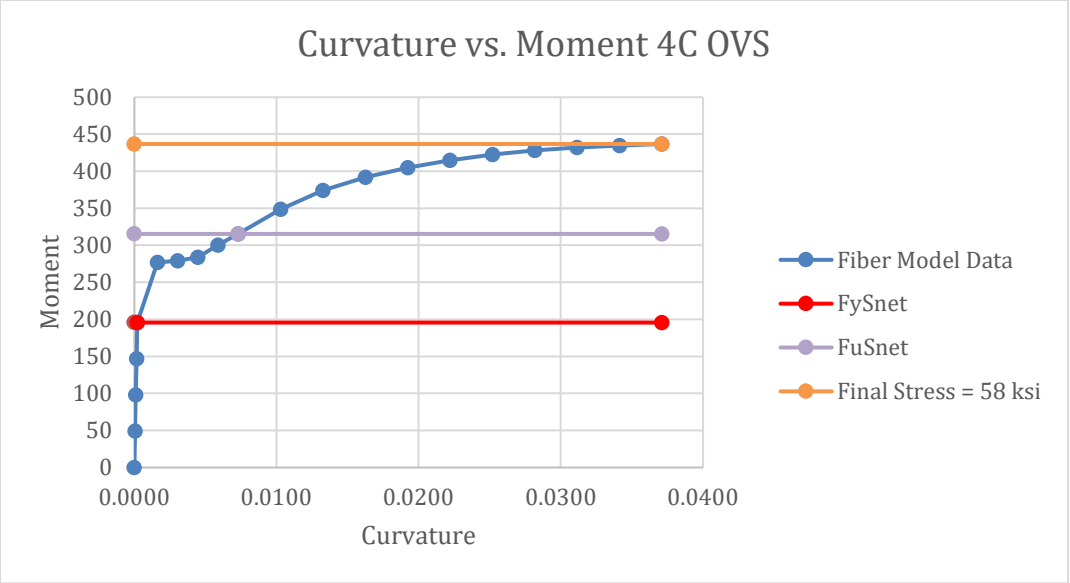
Curvature vs. Moment 4C OVS
Moment
Curvature
500
450
400
350
300
250
200
150
100
50
0
0.0000
0.0100
0.0200
0.0300
0.0400
Fiber Model Data
FySnet
FuSnet
Final Stress = 58 ksi

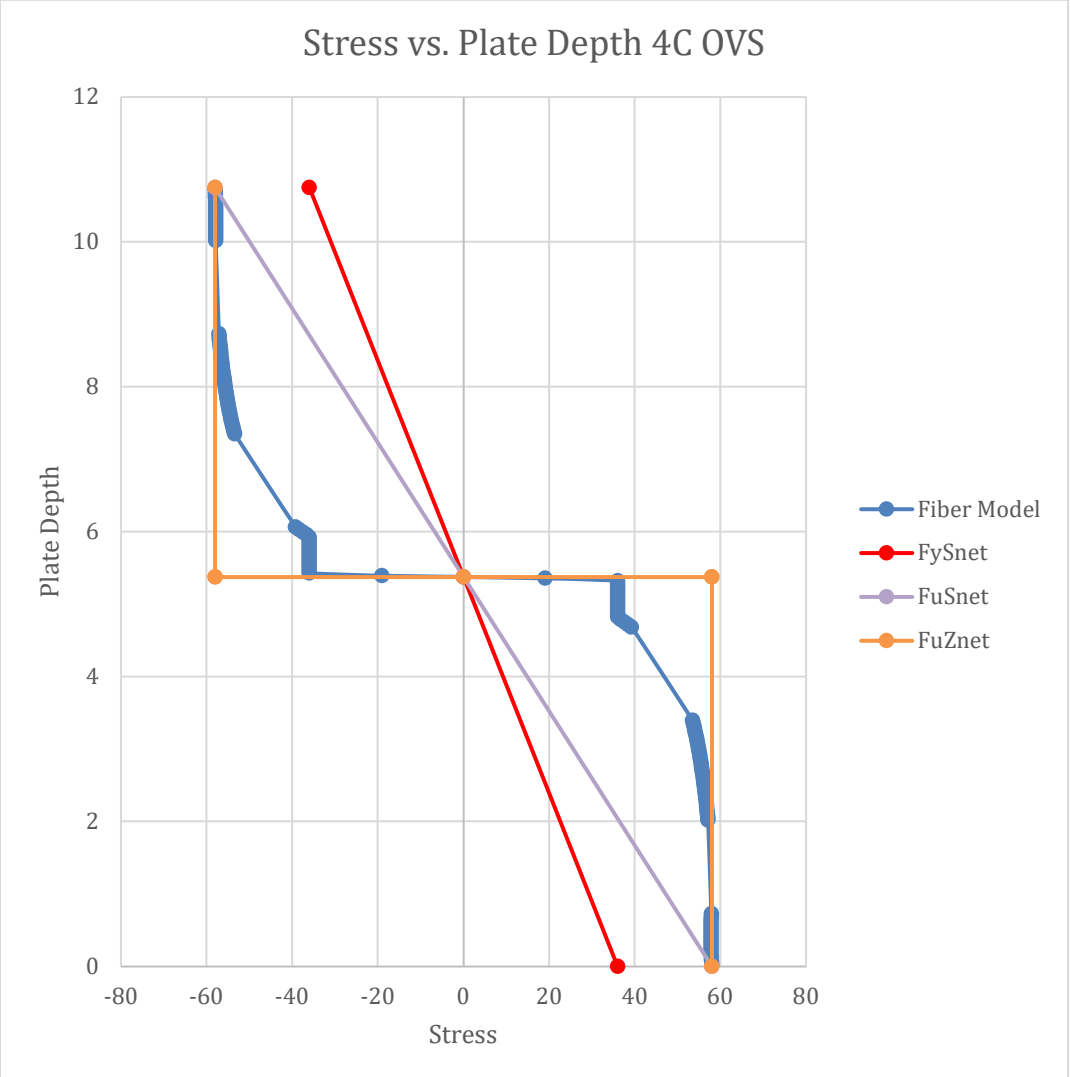
Stress vs. Plate Depth 4C OVS
Plate Depth
Stress
12
10
8
6
4
2
0
-80
-60
-40
-20
0
20
40
60
80
Fiber Model
FySnet
FuSnet
FuZnet

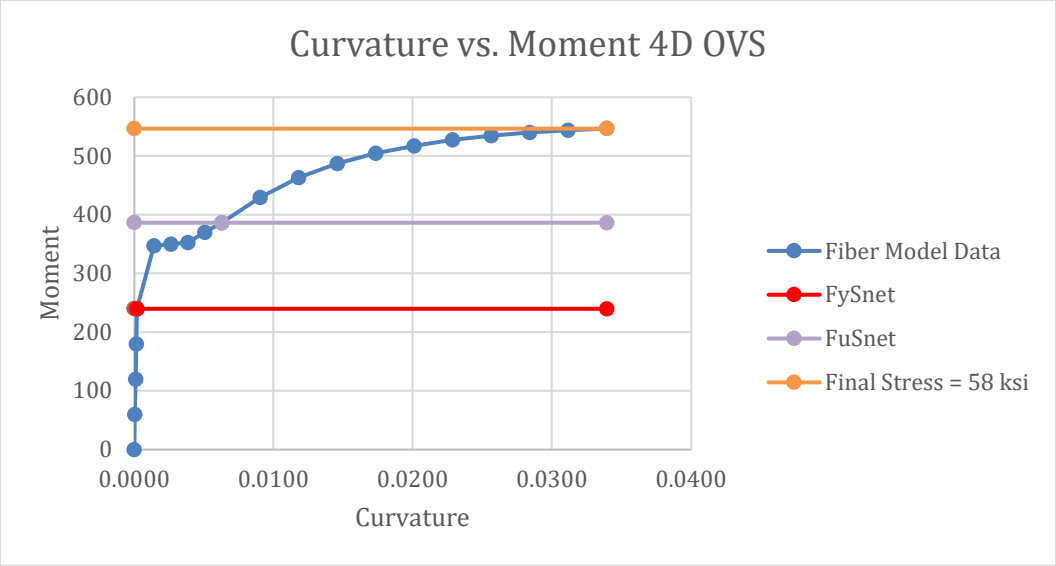
Curvature vs. Moment 4D OVS
Moment
600
500
400
300
200
100
0
0.0000
0.0100
0.0200
0.0300
0.0400
Curvature
Fiber Model Data
FySnet
FuSnet
Final Stress = 58 ksi

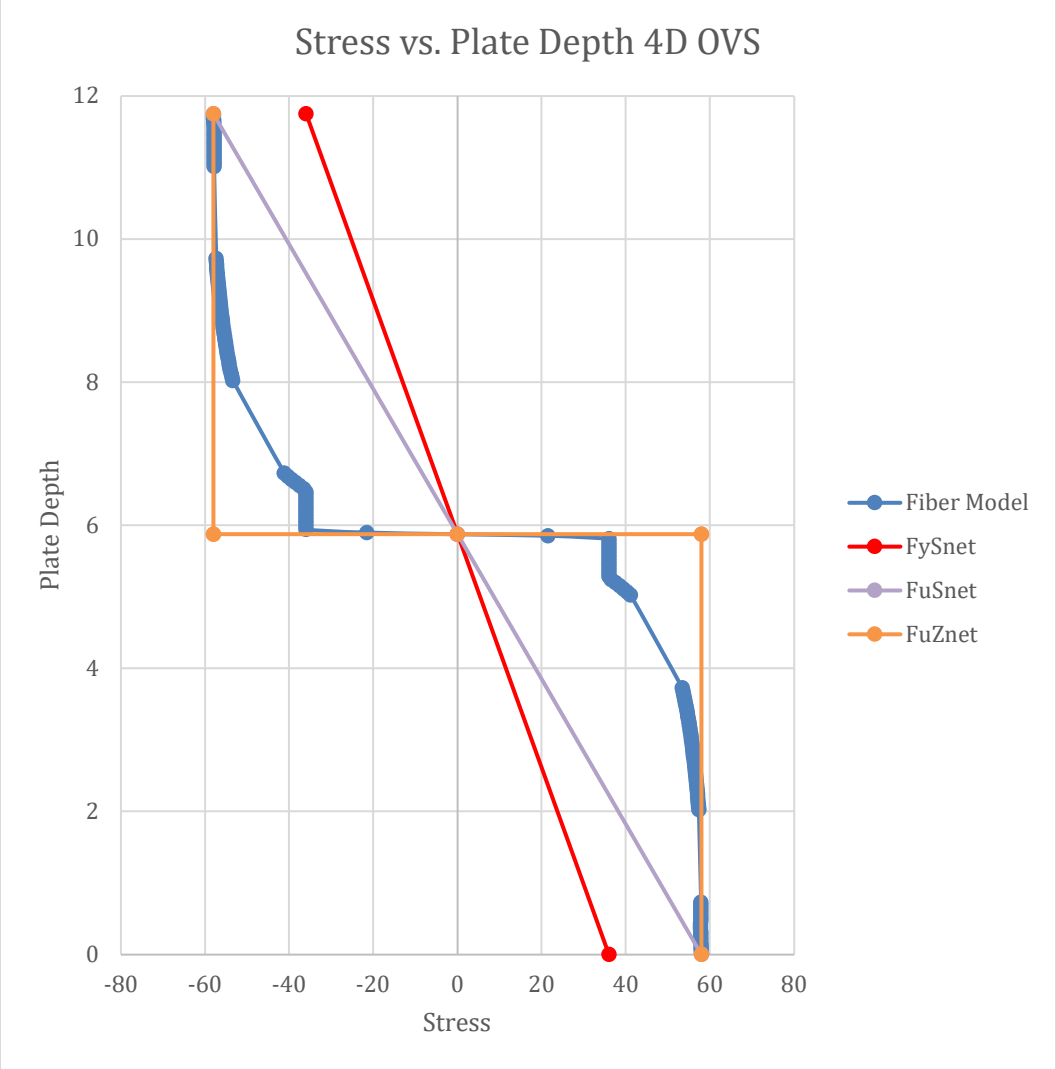
Stress vs. Plate Depth 4D OVS
Plate Depth
12
10
8
6
4
2
0
-80
-60
-40
-20
0
20
40
60
80
Stress
Fiber Model
FySnet
FuSnet
FuZnet

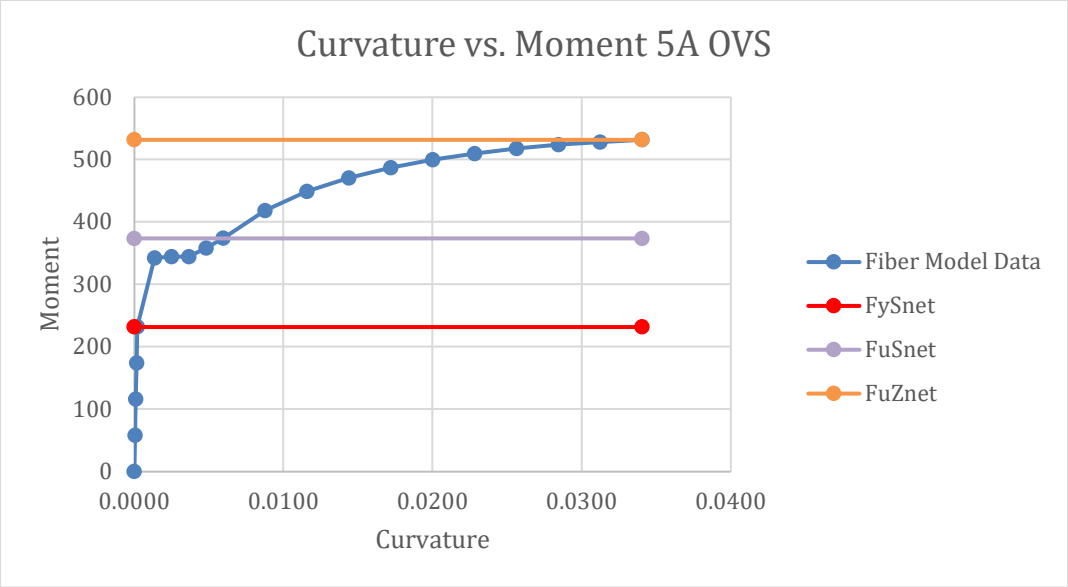
Curvature vs. Moment 5A OVS
600
500
400
300
200
100
0
Moment
0.0000
0.0100
0.0200
0.0300
0.0400
Curvature
Fiber Model Data
FySnet
FuSnet
FuZnet

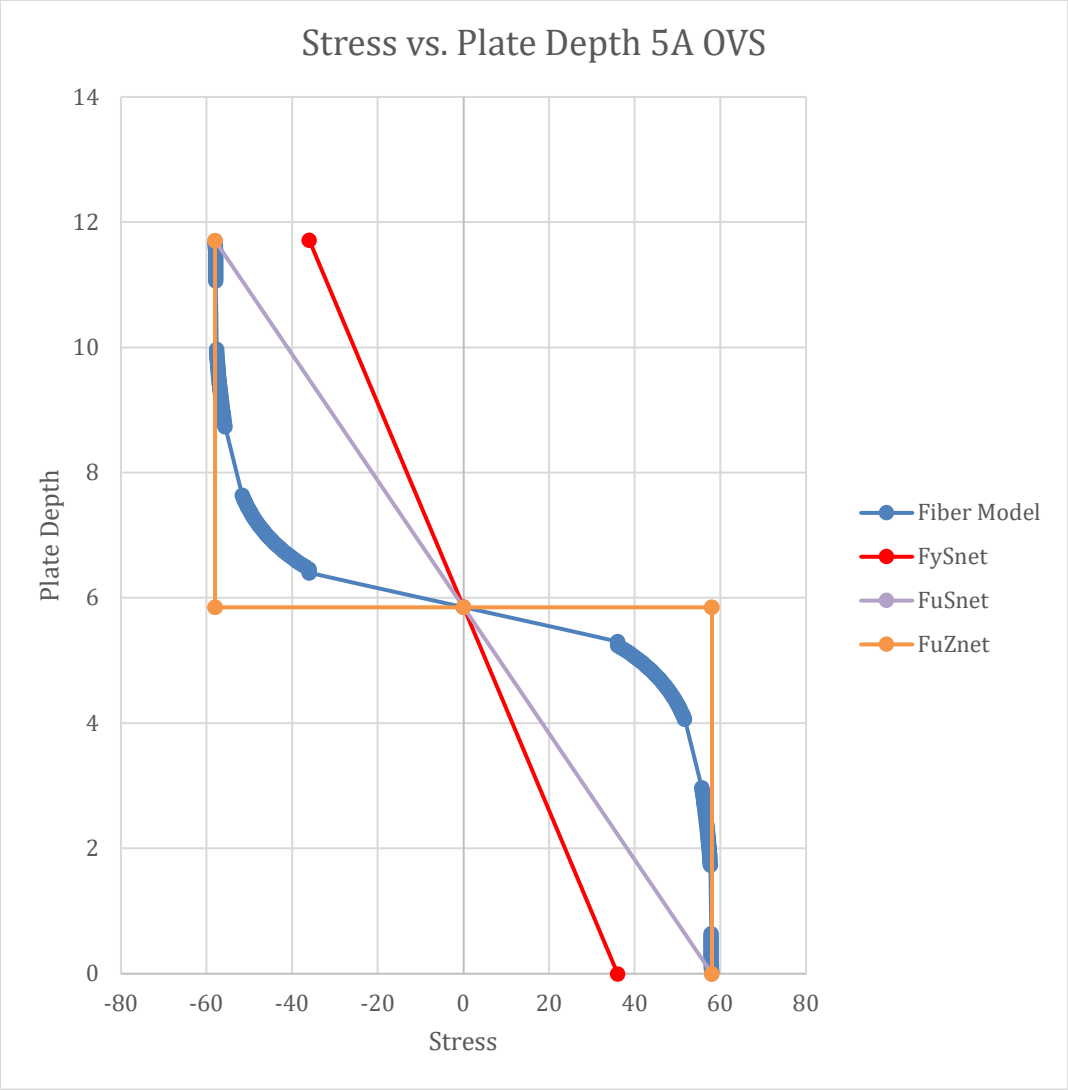
Stress vs. Plate Depth 5A OVS
14
12
10
8
6
4
2
0
Plate Depth
-80
-60
-40
-20
0
20
40
60
80
Stress
Fiber Model
FySnet
FuSnet
FuZnet

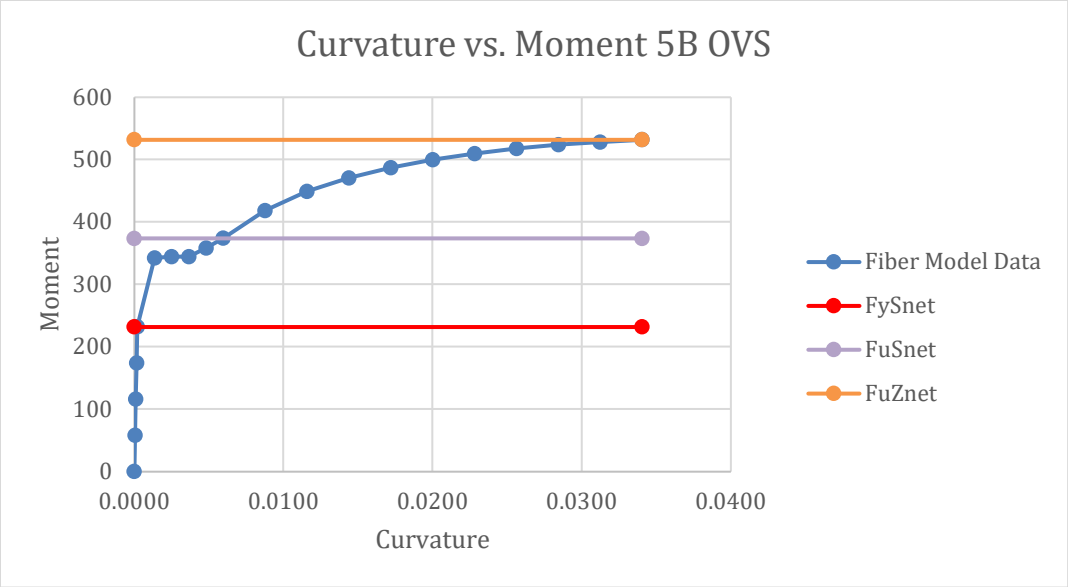
Curvature vs. Moment 5B OVS
600
500
400
300
200
100
0
Moment
0.0000
0.0100
0.0200
0.0300
0.0400
Curvature
Fiber Model Data
FySnet
FuSnet
FuZnet

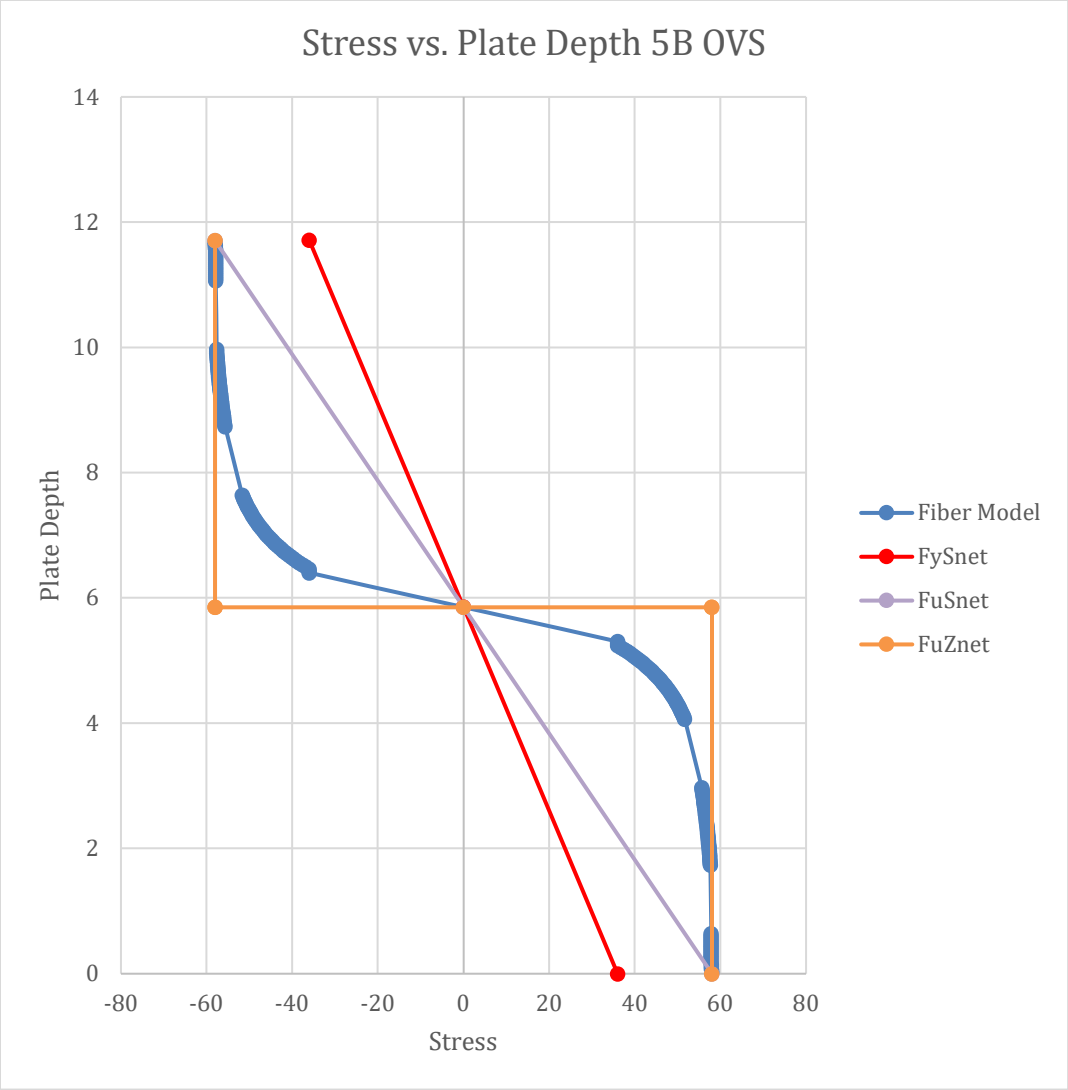
Stress vs. Plate Depth 5B OVS
14
12
10
8
6
4
2
0
Plate Depth
-80
-60
-40
-20
0
20
40
60
80
Stress
Fiber Model
FySnet
FuSnet
FuZnet

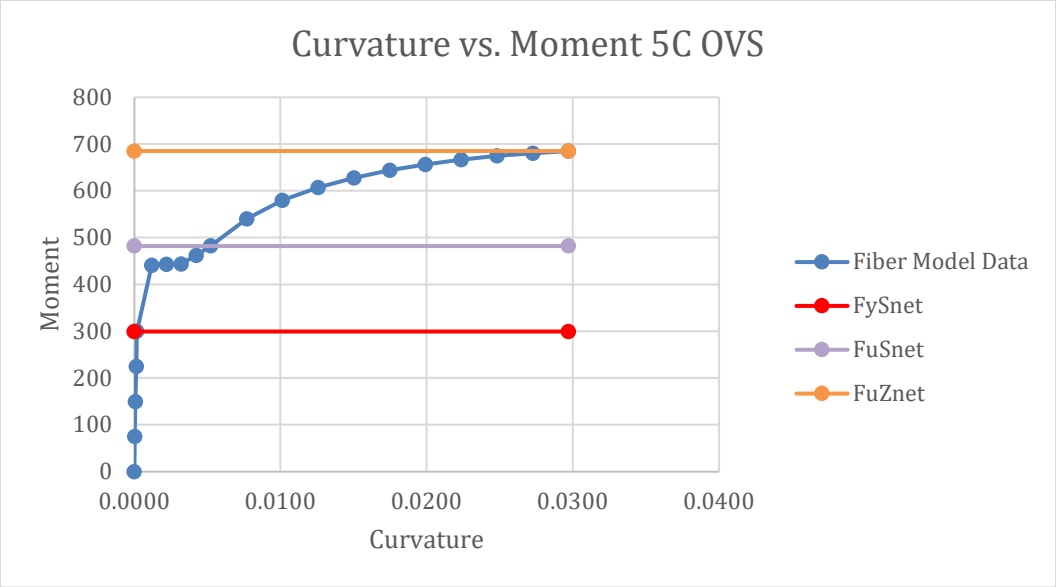
Curvature vs. Moment 5C OVS
800
700
600
500
400
300
200
100
0
Moment
0.0000
0.0100
0.0200
0.0300
0.0400
Curvature
Fiber Model Data
FySnet
FuSnet
FuZnet

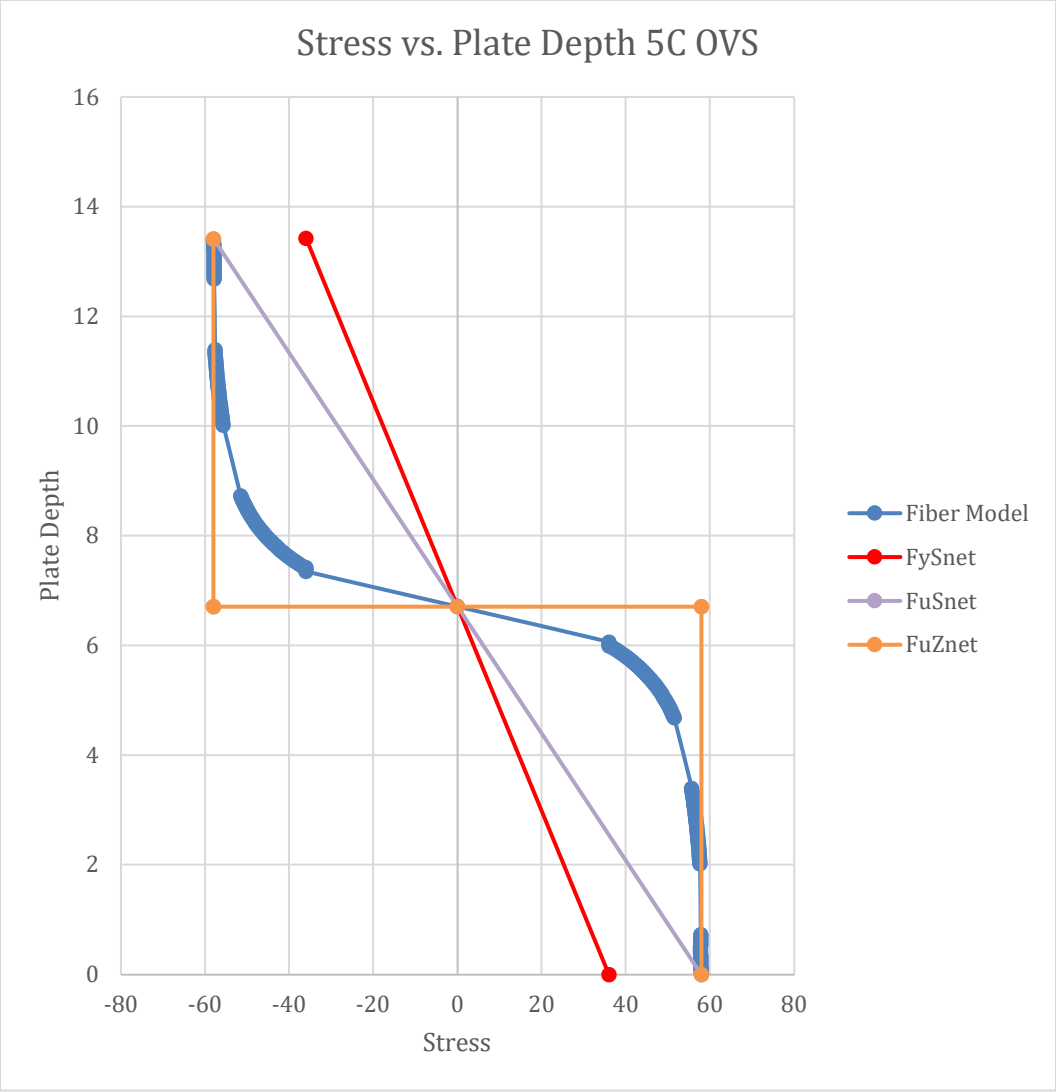
Stress vs. Plate Depth 5C OVS
16
14
12
10
8
6
4
2
0
Plate Depth
-80
-60
-40
-20
0
20
40
60
80
Stress
Fiber Model
FySnet
FuSnet
FuZnet

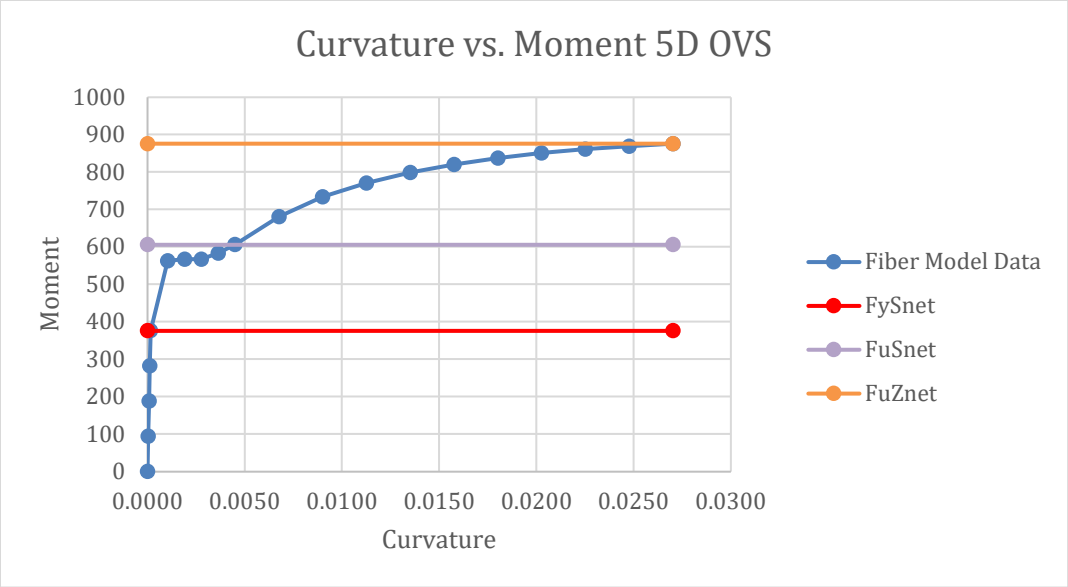
Curvature vs. Moment 5D OVS
Moment
1000
900
800
700
600
500
400
300
200
100
0
0.0000
0.0050
0.0100
0.0150
0.0200
0.0250
0.0300
Curvature
Fiber Model Data
FySnet
FuSnet
FuZnet

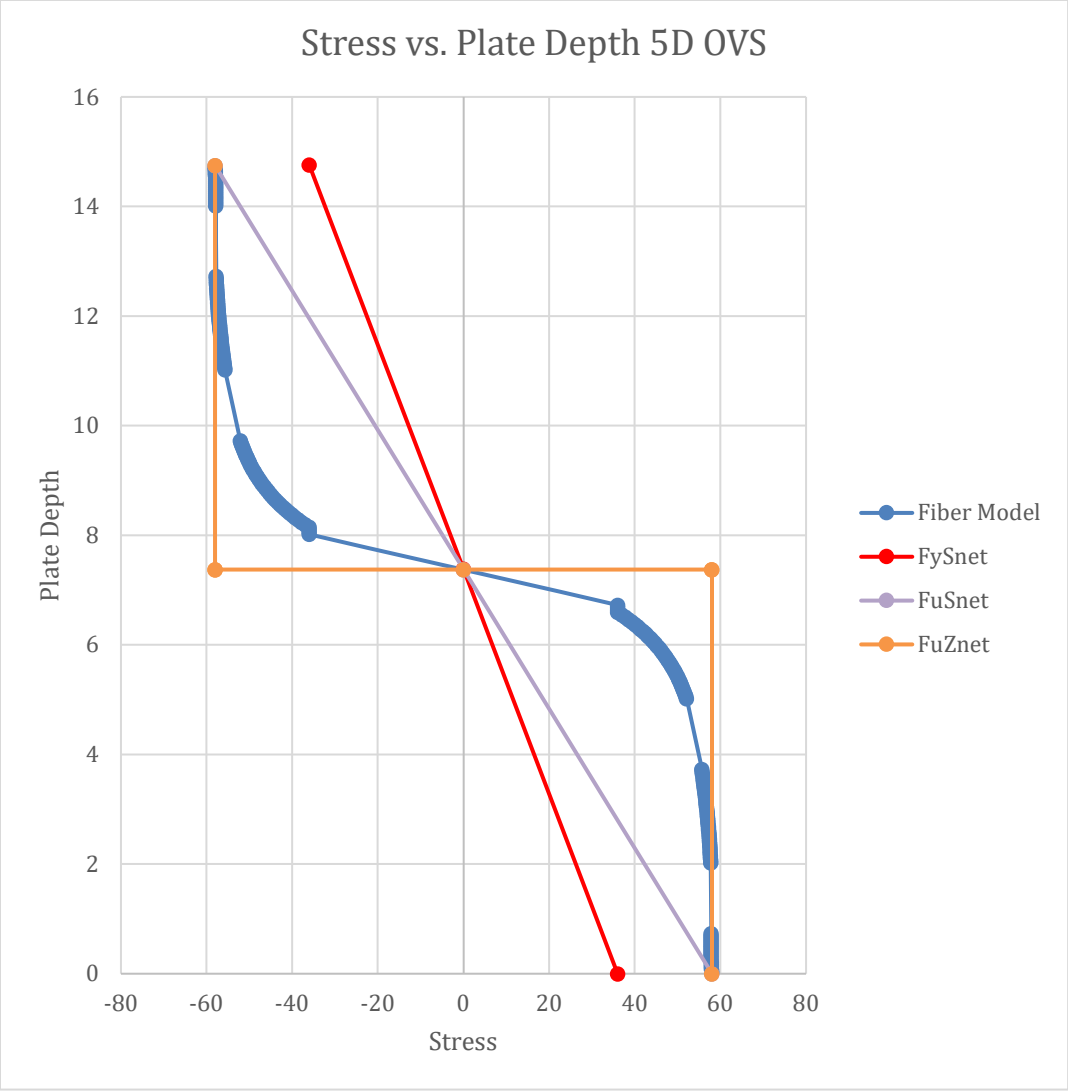
Stress vs. Plate Depth 5D OVS
Plate Depth
16
14
12
10
8
6
4
2
0
-80
-60
-40
-20
0
20
40
60
80
Stress
Fiber Model
FySnet
FuSnet
FuZnet